STRESS EVALUATION IN GRINDING PROCESS BY FINITE ELEMENT METHOD

by
M. GOPI KRISHNA

DEPARTMENT OF MECHANICAL ENGINEERING
INDIAN INSTITUTE OF TECHNOLOGY KANPUR
JUNE, 1983

STRESS EVALUATION IN GRINDING PROCESS BY FINITE ELEMENT METHOD

A Thesis Submitted
in Partial Fulfilment of the Requirements
for the Degree of
MASTER OF TECHNOLOY

by

M. GOPI KRISHNA

to the

DEPARTMENT OF MECHANICAL ENGINEERING
INDIAN INSTITUTE OF TECHNOLOGY KANPUR
JUNE, 1983

CERTIFICATE

This is to certify that the thesis entitled, ''Stress Evaluation in Grinding Process by Finite Element Method'' by M. Gopi Krishna, is a record of work carried out under our supervision and has not been submitted elsewhere for a degree.

K. Sri Ram
Professor,
Dept. of Mechanical Engineering,
Indian Institute of Technology,
Kanpur.

G.K. Lal
Professor,
Dept. of Mechanical Engineering,
Indian Institute of Technology,
Kanpur.

ACKNOWLEDGEMENT

The author wishes to express his deep sense of gratitude and appreciation to his advisors Dr. G.K. Lal and Dr. K. Sri Ram who has guided this work from conception to completion.

The author would like to thank his friends Satyanarayana, M.S. Prasad, Chandrasekar, Dr. E.S. Reddy, I.K. Bhatt, B.K. Dutta, Kamalakar, A.K. Srivastava, Murthy and many others, for their timely help provided whenever necessary.

Thanks are due to J.P. Gupta, V.P. Gupta, P.P. Singh to produce the work in the present form.

CONTENTS

LIST OF FIGURES AND TABLES

ABSTRACT

In the present work, temperatures and residual stress distributions in Plunge-cut grinding has been obtained using Finite Element Method. For simplicity, a two dimensional approximation for the grinding process is made. Transient heat conduction equation was solved to obtain the temperature distribution in the workpiece. The motion of the grinding wheel has been simulated by a step-by-step movement of the heat flux over the wheel-workpiece contact zone. The above temperature history has been used to find the residual stresses in the subsequent elastic-plastic analysis.

The numerical results obtained, confirms that the tensile residual stresses may reach the ultimate strength of the workpiece material. This causes grinding cracks whose presence reduces the fatigue strength of the ground part resulting in its premature failure. An increase in the depth of cut and/or the table speed results in increase of the peak value of the tensile residual stresses. Variation in heat transfer coefficient, so as to simulate the effect of cooling fluid, has marginal effect on the peak value of the tensile residual stress. The results so obtained compare well with the experimental data available in the literature.

CHAPTER I

INTRODUCTION AND LITERATURE REVIEW

1.1 INTRODUCTION

Grinding is a metal cutting process which is similar in many ways to other commonly employed methods of metal removal such as turning, milling or shaping. In grinding, material removal takes place due to shearing just as in other cutting operations. The grinding wheel may be described as a multi-toothed milling cutter, each tooth consisting of a small abrasive particle. Of all the metal cutting processes, grinding is undoubtedly the least understood. Because of the random grit geometry, high cutting speed, and small depth of cut taken in grinding, mechanisms of grinding are difficult to observe and evaluate.

The premature failure in service of components manufactured by the grinding process and the appearance of surface cracks during grinding of certain materials have made it an economic necessity to carry out detailed investigations into the surface integrity aspect of the process, including residual stresses. When a grain first contacts the workpiece surface (Fig. 1.1), sliding and ploughing occurs. As the grain moves it experiences more and more uncut material and the forces required to remove this material increase, and

ultimately the material is removed in the form of a chip. During this process of material removal, large amount of heat is generated in the workpiece, due to plastic deformation of the work material, due to frictional sliding of the grain over the workpiece surface, and due to the rubbing action between the chip and the grain. Most of the heat generated (about 80-85%) enters the workpiece and the resulting temperature rise may cause burn or thermal cracks on the workpiece surface. The above process of material removal leads to inhomogeneous plastic deformation. Therefore, individual elements of the workpiece undergo different changes in their dimensions. Besides the forces in the workpiece, which are in equilibrium with the applied forces, additional forces maintain equilibrium within the workpiece after the release of external loadings. These internal forces cause stresses which are called residual stresses.

The residual stresses can have three different origins :

(1) Forces between the workpiece and the tool

The forces in a cutting process cause elastic and plastic deformation. The elastic deformation subsides as soon as the cutting process terminates. The plastic deformation remains and results in compressive residual stresses in the workpiece surface.

(2) Heat Expansion

The material expands locally owing to the heat generated during the cutting process. If the cutting temperatures are too high, inhomogeneous expansion will exceed the limits of elastic deformation of the material and leads to tensile residual stresses after cooling. In extreme cases, cracks can appear on the workpiece surface.

(3) Structural Transformation

Grinding temperature, sometimes reaches the hardening temperature of the material. Because of the temperature gradient, tempering occurs in certain layers below the surface, while the workpiece surface is rehardened by virtue of reaching the critical cooling speed through the application of coolant liquid. The tempered material has a smaller volume compared with the original lattice, whereas the newly-hardened workpiece material reverts to same volume as before. Tensile residual stresses are thereby created.

Under fine grinding conditions, the temperatures developed are well below the temperature that leads to structural transformation. The possibility of residual stresses due to this transformation is therefore negligible. The effect of mechanical loading on residual stresses were studied by Mishra et al. [17], and it is found to be negligible.

Residual stresses are therefore mainly due to non-uniform temperature distribution in the workpiece, generated during grinding.

The thermal gradients that are imposed on the uppermost layers of the body would result in a large thermal expansion. Becuase of the deformation constraints created by the much stiffer and not thermally affected material of the workpiece, large compressive stresses are built up during heating-up period, which may surpass the yield limit of the material, especially at elevated temperatures. During cooling down period, the upper layer tends to contract elastically more than the substrate, creating tensile residual stresses in the uppermost layer.

Residual stresses are detrimental to the fatigue life of the ground part. Previous studies have indicated that compressive residual stresses increase the fatigue strength of ground parts. Since grinding operation is the last process to be performed over the part, the stresses that are created during this process determines the life of the part.

1.2 LITERATURE SURVEY

GRINDING TEMPERATURES

The first attempt to estimate the grinding temperatures appears to have been made by Guest [1]. He proceeded with the

assumption that half of the total heat generated passes away with the chips and related the specific horsepower to the temperatures. But due to the complexity of the process and difficulties involved in measuring the temperatures accurately, analytical approaches have been resorted to. These temperatures models [2-4] employed the moving heat source theory proposed by Jaeger [5]. Shaw et al. [2] used this theory, with the assumption, that an average grit on the wheel surface has a rake angle of zero degree, and estimated the workpiece surface temperatures for the fine surface grinding. They also measured the temperatures experimentally, and concluded that as table speed increases, temperature increases. Sato [6], determined the temperature at the wheel-work contact surface from the heat quantity conducted into the workpiece, which he found out analytically. His theory was based on the assumption that the workpiece is a semi-infinite body and the grinding wheel is an instantaneous heat source. He also found out that 85% of the grinding energy is conducted as heat into the workpiece. Des Ruisseaux and Zerkle [3] calculated the grinding temperatures as the sum of a local temperature due to grinding by an individual grain, and a grinding zone temperature due to grinding by all other grains. The relations were established by considering the grinding geometry. Malkin and Anderson [7] considered the total grinding energy as composed of energy required for chip formation, ploughing and sliding. He assumed that a portion

of this energy is conducted as heat into the workpiece and related these results to grinding temperatures and workpiece burn. Sauer [8], in his theory combined both experimental and analytical techniques, and calculated the temperatures. The effect of coolant and rise in temperature due to plastic deformation was considered.

RESIDUAL STRESSES

Several researchers have attempted to determine residual stresses experimentally. A considerable portion of the work is attributed to Gilkman and Stepnov [9], Frisch and Thomsen [10], Marshell and Shaw [11], Letner [12,13], Colwel, Sinnot and Tobion [14], Halverstadt [15] and others. A review of existing experimental work brings out two main aspects. Firstly the experimental determination is often done by bending-deflection method. This method involves removing of material from the stressed surface electro-chemically or by etching, whilst measuring the curvatures at regular intervals using a sensitive measuring device. This method is beset with difficulties in controlling the uniformity of layer removed, and accurate measurement of curvature of the specimen, which effects the stresses calculated. Secondly, the stress distribution is influenced by a number of grinding parameters such as wheel speed, wheel grade, depth of cut etc., besides the metallurgical nature of the material being ground. Both tensile and compressive residual stresses

have been found near the surface under different sets of conditions, and published data are often contradictory. Thus it is difficult to form a clear picture as to the influence of processing parameters on the residual stresses introduced.

Other methods that have been employed for estimating the residual stresses are X-ray diffraction method, Sachs boring method etc. [16]. The measurement of residual stresses by X-ray, utilises the interatomic spacing of surface lattice planes as the guage length for measuring strain. Using Bragg's law, which expresses the relationship between the distance from each other of a given set of lattice planes, the wavelength of X-ray diffraction, the order of diffraction, and the measured diffraction angle, the usual stress equation for the two-exposure technique is given by

$$S = \frac{E}{1+\nu} \frac{\Delta\theta}{\sin^2\psi \tan\theta} = K\Delta\theta$$

where

$\Delta\theta$ = change in the Bragg angle between normal and inclined exposures

K = constant

This method is particularly useful, where surface stresses are important, and since the exposure area is small, steep stress gradients can be obtained. But the disadvantage is that the equipment is expensive, and if the area to be examined is large, then measurements are tedious. This method is inapplicable to specimens that have been subjected to uniaxial plastic deformation and difficult to apply to heat-treated high-tensile steels and severely cold worked materials.

Sach's boring method employs the technique of boring out a cylinder or tube in stages and measuring longitudinal and circumferential strains at the outer surface caused by the release of residual stresses. The assumptions involved in this method are, material is isotropic and Youngs modulus, Poisson's ratio are constant, residual stresses are distributed with rotational symmetry about the axes, the tube formed by boring is circular in section and the inner and outerwall surfaces are concentric, specimen is sufficiently long to prevent lateral bending. The disadvantage over the bending deflection technique is that plastic deformation should not occur on layer removal, strain guages used must be highly sensitive.

The residual stress distribution has been obtained analytically by Mishra et al. [17] using Finite Element Method. They have obtained the temperature distribution in the body, from the relation given by Jaeger [5], and proceeded to obtain

stresses using elasto-plastic analysis. No attempt was made to evaluate the effect of grinding variables on residual stresses, and comparison with the experimental values.

1.3 FINITE ELEMENT TECHNIQUE

In many practical situations, the geometry of the system and the boundary conditions are too complex to yield analytical solutions. Such problems can, however be solved by numerical methods. Popular amongst these numerical techniques are Finite Difference and Finite Element Methods. The Finite Difference scheme of a problem gives a pointwise approximation to the governing equations. The accuracy of this model can be increased by taking more number of grid points, but its main drawback is, it becomes hard to apply this technique for problems with irregular geometries or unusual specifications of the boundary conditions. Whereas Finite Element Method envisions the solution region as built up of many small interconnected sub-regions or elements. This method gives a piecewise approximation to the governing equations. The basic premise of the Finite Element Method is that a solution region can be analytically modelled or approximated by replacing it with an assemblage of discrete elements. Since these elements can be put together in a variety of ways, they can be used to represent exceedingly complex shapes.

In more and more engineering situations today, it is necessary to obtain approximate solutions to the problems rather than exact closed form solutions. The Finite Element Method is a numerical analysis technique for obtaining approximate solutions to a wide variety of Engineering problems.

In a continuum problem of any dimension, the field variable (whether it is pressure, temperature, displacement, stress, or some other quantity) possesses infinitely many values because it is a function of each generic point in the body or solution region. Consequently, this problem is one with an infinite number of unknowns: The finite element discretization procedure reduce the problem to one of a finite number of unknowns by dividing the solution region into elements and by expressing the unknown field variables in terms of assumed approximating functions within each element. The approximating functions (sometimes called interpolation functions) are defined in terms of the values of the field variables at specified points called nodes or nodal points. The nodal values of field variable and the interpolation functions for the elements completely define the behaviour of the field variable within the elements. The nature of the solution and the degree of approximation depends not only on the size and the number of elements used, but also on the interpolation function selected. A Finite Element Model of a problem gives a piecewise approximation to the governing equations. The important feature

of the Finite Element Method is its ability to formulate solutions for individual elements before putting them together to represent the entire problem.

The various steps involved in the solution of a problem using Finite Element Method are :

(1) Discretization of continuum,
(2) Selecting interpolation functions,
(3) Finding the element properties,
(4) Assembling the element properties to obtain the system equations,
(5) Solve the system equations,
(6) Make additional computations for stress/strain evaluation.

1.4 PRESENT WORK

A frequent cause of failure of ground surfaces is a network of practically invisible cracks that develop during or immediately after grinding as a result of considerable heat generated during the process, and the presence of high residual stresses in the ground surface. If the tensile residual stresses produced by grinding are high enough to exceed the rupture strength of the material, cracks will form under the operational loads to which the surface is subjected, this crack propagates leading ultimately to the failure of the part.

In the present work, an attempt has been made to study the effect of grinding parameters on the temperatures generated and the residual stresses thus formed. For simplicity, a two dimensional case for plunge cut grinding has been considered. Temperatures were obtained by solving the basic heat conduction equation in a solid using Finite Element Method. The cooling effect is introduced as a specific thermal boundary condition at the workpiece surface. An iterative procedure is employed for the step-by-step movement of the temperature field, in order to simulate the movement of the grinding wheel over the workpiece surface. Since the residual stresses are mainly due to non-uniform temperature distribution in the workpiece an attempt has been made to obtain the elastic-plastic stress field within the workpiece from the temperatures calculated above. The results obtained using this approach have been compared with the available experimental data.

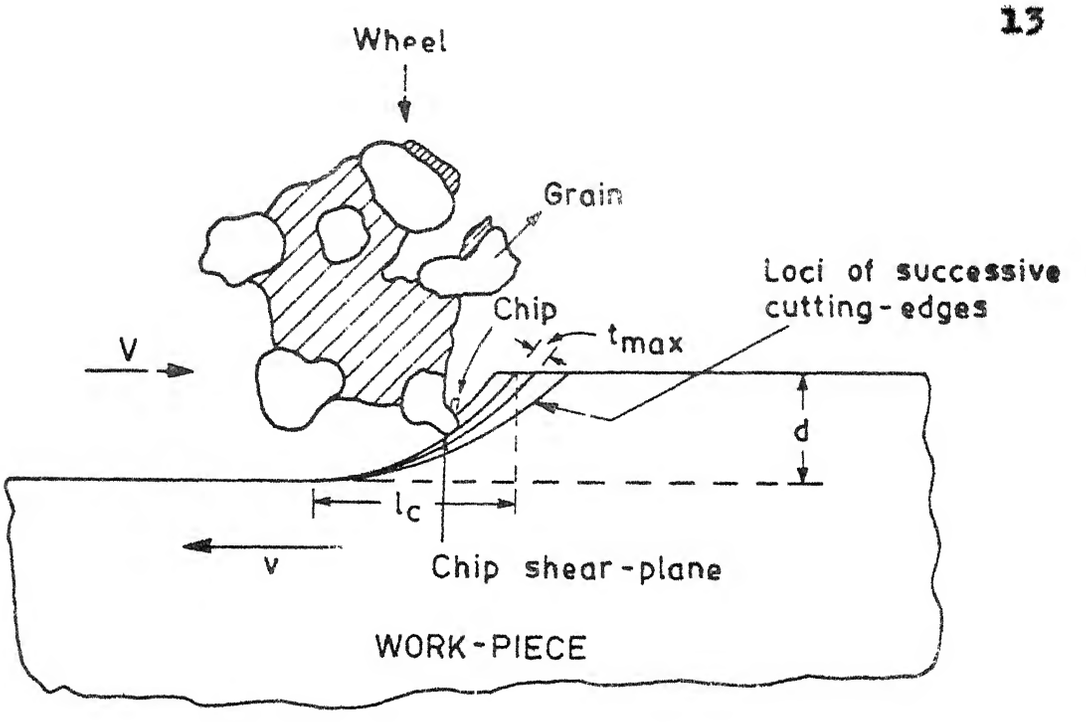

Fig. 1.1 Chip formation process in grinding.

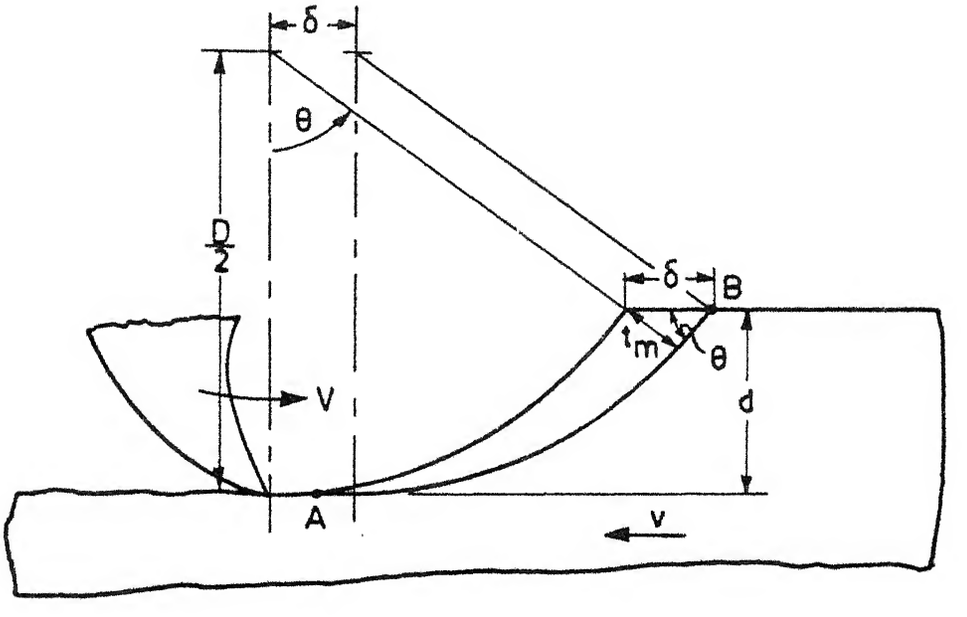

Fig. 1.2. Approximate shape of plain milling chip.

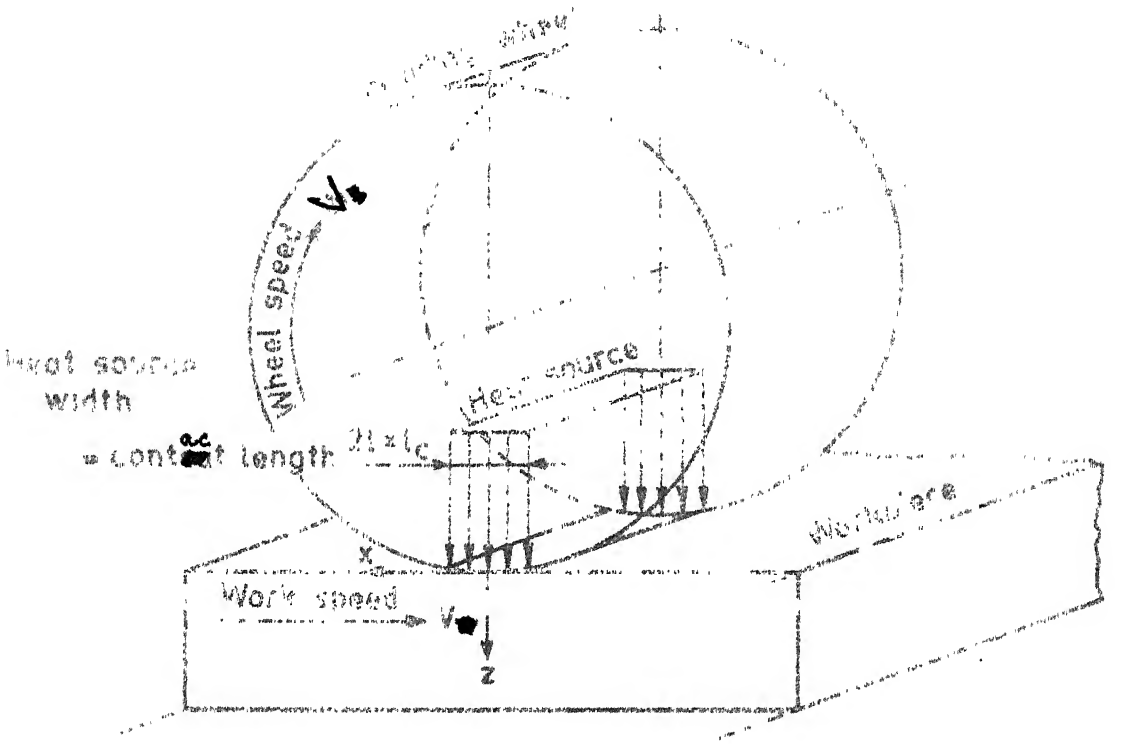

Fig. 1.3 Two dimensional thermal model representing grinding action.

CHAPTER II

THERMAL ANALYSIS

2.1 INTRODUCTION

A large percentage of energy used in grinding is transformed into thermal energy which causes the workpiece temperature to increase. For obtaining better grinding results, it is necessary to minimise this temperature rise because of the following :

(1) The maximum temperature in the contact area between the wheel and the workpiece determines the rate of chemical reaction at the interface.

(2) The maximum temperature of a finished workpiece surface determines the integrity (or micro structural damage) of the surface.

(3) The average temperature of the bulk of the workpiece determines the dimensional accuracy after grinding.

Most of the theoretical models for obtaining grinding temperatures are either based on Jaeger's band source model or moving line source model [5]. In Jaeger's thermal model, a band heat source is assumed to move on the workpiece surface at a speed equal to that of the workpiece velocity v. Based on this model Des Ruisseaux and Zerkle [3] calculated the surface

temperatures by superimposing the temperatures due to a single grain and due to all other grains in the contact zone. Sauer's analysis [8] also considered the heat input due to plastic deformation of the workpiece but this heat due to plastic deformation is often of secondary importance. Sato's theory [6] was based on the temperature rise of the surface of a semi-infinite body under an instantaneous heat source. He calculated the heat generated during grinding from the tangential grinding forces.

2.2 ANALYSIS

The temperature model is characterised by three sets of fundamental physical quantities. (1) The heat input into the workpiece and its distribution over the contact area, (2) the real contact length (l_c) and (3) the thermal characteristics of metal (conductivity k, specific heat per unit volume ρc).

(1) Actual heat input

The fraction of the total energy dissipated by the heat source flowing directly into the workpiece is of special importance from the point of view of thermal load on the workpiece. This was experimentally measured by several authors [6,7,8]. Roughly 70-90% of the total consumed energy flows instantaneously into the workpiece causing a rapid increase in the local workpiece temperature. A large specific metal

removal rate usually reduces this percentage but blunt wheels show a tendency of increasing this value [7]. In the present work, it is assumed that 80% of the total energy dissipated by the heat source flows into the workpiece instantaneously.

(2) Contact length

The real contact length l_c is a function of wheel dimensions, composition and characteristics. It also depends upon the kinematic parameters (speeds and forces) because they govern the normal grinding force component and elastic flattening of the wheel in the contact area. The length l_c is approximately equal to

$$l_c = \sqrt{Dd} , \qquad (2.1)$$

where

D = effective wheel diameter (mm)

d = depth of cut (mm)

The width of the interference zone is equal to the width of contact between the wheel and the workpiece. For plunge cut grinding it is equal to the width of the workpiece.(Fig. 2.1). Heat flux distribution in the grinding wheel-work interface has been studied by Jaeger [5] and Sauer [8]. They found that this flux distribution has effect upon the maximum temperatures developed during grinding. Further, only a few

microns below the ground surface are most affected by the shape of the flux distribution. So a uniform heat distribution may be assumed for the evaluation of temperatures without affecting very much the overall accuracy of the results.

(3) Thermal characteristics

The thermal characteristics of workpiece material, in general, are temperature dependent. However, an adequately chosen average value may give a fairly good approximation of the temperature distribution as reported by Sauer [8]. This assumption simplifies the solution of the heat transfer equation for evaluating the temperatures using Finite Element Model.

The temperature rise in the workpiece can be calculated by approximating the combined action of all grains and by considering the wheel as a single heat source moving with a velocity, v, over the workpiece. The bulk temperature rise in the workpiece due to one pass of grinding wheel, assumed initially to be at uniform temperature, T_o, is obtained from the temperature rise due to interference zone surface heat source.

The interference zone heat flux is given by [8]

$$\dot{Q}_F = \frac{\alpha F_p V}{B l_c J} , \qquad (2.2)$$

where

α = fraction of the total grinding energy entering into the workpiece

F_p = horizontal grinding force (gmf)

V = wheel speed (mm/sec)

B = width of the workpiece (mm)

J = Joules constant (gmf-mm/cal)

Newtonian cooling at a uniform rate h (cal/mm^2-sec-^oC) from the surface is assumed for calculating bulk temperatures.

Two dimensional transient heat conduction equation, for a uniformly thick workpiece of thickness t is given by [18]

$$\frac{\partial}{\partial x}\left(k_x \frac{\partial T}{\partial x}\right) + \frac{\partial}{\partial y}\left(k_y \frac{\partial T}{\partial y}\right) + Q - \rho c \frac{\partial T}{\partial \tau} = 0. \quad (2.3)$$

The desired temperature must satisfy the following boundary conditions :

(a) $T = T(x,y,\tau)$ on S_1, $\tau > o$ (Fig. 2.2)

(b) $k_x \frac{\partial T}{\partial x} n_x + k_y \frac{\partial T}{\partial y} n_y + \dot{Q}_F + h(T-T_\infty) = 0$ on S_2, $\tau > o$

(c) $T = T_o(x,y)$ in D, $\tau = o$

where

k_x, k_y = thermal conductivities in x and y directions, respectively (cal/mm-sec-^oC)

Q = internal heat generation

T_o = initial temperature in the domain (^oC)

$T(x,y,\tau)$ = specified boundary temperature distribution (^oC)

n_x, n_y = direction cosines of the outward drawn normal vector $\bar{n}$ to the bounding curve

$\dot{Q}_F$ = heat flux lost or added at the boundary due to conduction ($cal/sec\text{-}mm^2$)

$h(T-T_\infty)$ = heat lost at the boundary due to convection to ambient temperature, T_∞, with convective heat transfer coefficient h

ρ = density of the workpiece material (gm/mm^3)

c = heat capacity of the material ($cal/gm\text{-}^oC$)

Equation (2.3) in its variational form can be written as

$$\chi = \int_o^t \iint_S \left[\tfrac{1}{2} k_x \left(\frac{\partial T}{\partial x}\right)^2 + \tfrac{1}{2} k_y \left(\frac{\partial T}{\partial y}\right)^2 - QT + T\, \rho c \frac{\partial T}{\partial \tau}\right] dS\,dZ$$

$$+ \int_o^t \dot{Q}_F\, T\, dB\,dZ + \int_o^t \int \left(\tfrac{1}{2} h T_\infty^2 - h T_\infty T\right) dB\,dZ . \qquad (2.4)$$

The entire continum is discretized into a finite number of sub-regions as shown in Fig. 2.2. Minimisation of this functional requires an explicit formulation of temperature T in each element.

Assuming the temperature distribution within each element as

$$T^{(e)}(x,y,\tau) = \sum_{i=1}^{r} N_i(x,y)T_i(\tau) = [N(x,y)]\ \{T(\tau)\}^{(e)}, \tag{2.5}$$

where

r = number of nodes assigned to each element,

T_i = discrete nodal temperatures,

$N(x,y)$ = shape functions or interpolation function.

The functional has a minimum, when its first variation with respect to T vanishes. The resulting equations in the matrix form can be written as [19]

$$\int\int_{S^{(e)}} [k_x \{N_{,x}\}\ [N_{,x}] + k_y \{N_{,y}\}[N_{,y}]]dxdy\ \{T\}^{ne} +$$

$$\int\int_{S^{(e)}} \rho c \{N\}[N]\ dxdy \{\dot{T}\}^{ne} = \{Q\}^{(e)} - \{\dot{Q}_{FL}\}^{(e)}$$

$$- [k_n]\ \{T\}^{ne} + \{k\ T_\infty\}^{(e)}, \tag{2.6}$$

where superscript e refers to the element considered and $N_{,x}$, $N_{,y}$ are the partial derivatives of the shape function or interpolation function. After subsequent integration over each element and assembling all the element matrices, to form the global matrix, leads to a system of first order differential equation. This can be represented in matrix form as

$$[K_C]\{\dot{T}\} + [K_{TH}]\{T\} = \{Q\} - \{\dot{Q}_{FL}\} - [K_H]\{T\} + \{KT_\infty\}, \tag{2.7}$$

where

$[K_C]$ = thermal capacitance matrix,

$[K_{TH}]$ = thermal conductivity matrix,

$\{Q\}$ = internal heat generation,

$\{\dot{Q}_{FL}\}$ = heat loss or gain due to conduction,

$[K_H] = \oint_{S_1} h\{N_B\}[N_B]\, dB$ Heat loss due to convection

$[K_T] = \oint_{S_2} h\, T_\infty\{N\}\, dB$ on the boundary,

N_B = interpolation functions, on the boundary.

The boundary conditions that were considered in the present case are, cooling at a uniform rate by convection with convective coefficient h (cal/mm^2-sec-^oC) from the surfaces AB, BC and AD (Fig. 2.3). The surface DC is insulated so that no heat can pass through the workpiece into the magnetic chuck on which the workpiece is mounted.

The boundary conditions are then substituted and the resulting first order differential equations are solved using Crank-Nicholson recurrence relation giving [20]

$$\left(\frac{2}{\Delta\tau}[K_C]+[K_{TH}]\right)\{T_\tau\} = \left(\frac{2}{\Delta\tau}[K_C]-[K_{TH}]\right)\{T_{\tau-\Delta\tau}\} - (\{F_\tau\}+\{F_{\tau-\Delta\tau}\}), \tag{2.8}$$

where F is the R.H.S. of the equation (2.7). Here it is assumed that the temperature varies linearly with time during the arbitrary time interval $\Delta\tau$. The time interval $\Delta\tau$ is obtained in the following manner.

The movement of grinding wheel is approximated such that, it moves in discrete steps. The time for which the interference zone heat flux is acting on the workpiece, i.e., the time required for the wheel to travel between two successive steps is

$$\tau_{int} = \frac{l_c}{v} \quad . \tag{2.9}$$

For this time period, it is assumed that the heat flux is stationary. This time period is suitably divided into a number of time intervals $\Delta\tau$, and equation (2.8) is solved. After the time period τ_{int}, the wheel is shifted to a distance l_c (i.e. the heat flux zone is shifted) and then equation (2.8) is again solved for a period τ_{int} using the temperature obtained in the preceding case. This process is continued till the contact between the wheel and the workpiece ceases. Thus the temperature history in the workpiece is obtained, as the wheel proceeds.

2.3 COMPARISON WITH EXPERIMENTAL RESULTS

A computer programme was developed to solve equation (2.7) by the recurrence relation given in equation (2.8), and

the grinding temperatures were obtained for different sets of conditions. The model was tested by comparing with the experimental results obtained by Sauer [8]. A close agreement between the theoretical and experimental results is obtained. A typical temperature distribution curve is shown in Fig. 2.15. The input data used is given in Table 2.1A.

2.4 NUMERICAL RESULTS

For the present work, the data was taken from the experimental work of Pande and Lal [21] and is tabulated in Table 2.1B. The resulting temperature distributions, are shown in Figs. 2.4 to 2.14. From Fig. 2.4, it can be seen that the maximum temperature attains a constant value, and as the wheel moves over, a wake of temperature field is left behind. The temperature distribution in the contact length (l_c) shows a steep increase to the peak value and then drops rapidly, confirming the theoretical predictions of Jaeger [5]. The peak temperature shifts to the rear of the heat source length, as the contact length increases. This is also in accordance with Jaeger's model.

The temperature distribution inside the workpiece at various depths from the surface is shown in Fig. 2.6. As the depth is increasing, the peak temperature shifts towards the rear side of the heat source length. Fig. 2.7 to 2.14 show the plots of temperature distribution for

various depth of cuts and table speeds. As the table speed increases, there appears to be a slight increase in the peak temperatures, Fig. 2.17 , but at lower table speeds the depth of heat affected zone increases. This is shown in Figs. 2.6 to 2.8.

The effect of depth of cut is more pronounced on the temperatures. As the depth of cut increases, the peak temperatures increase significantly. These are shown in Figs. 2.8-2.10.

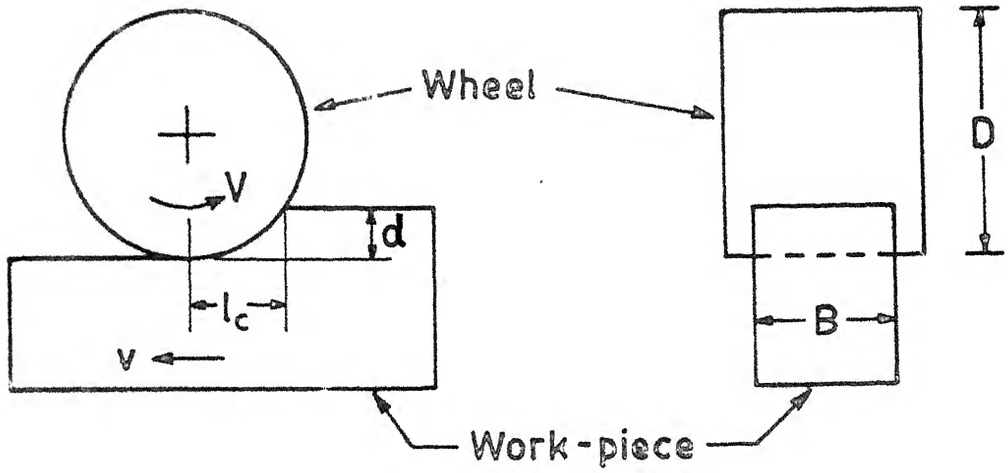

Fig. 2.1 Plunge cut surface grinding.

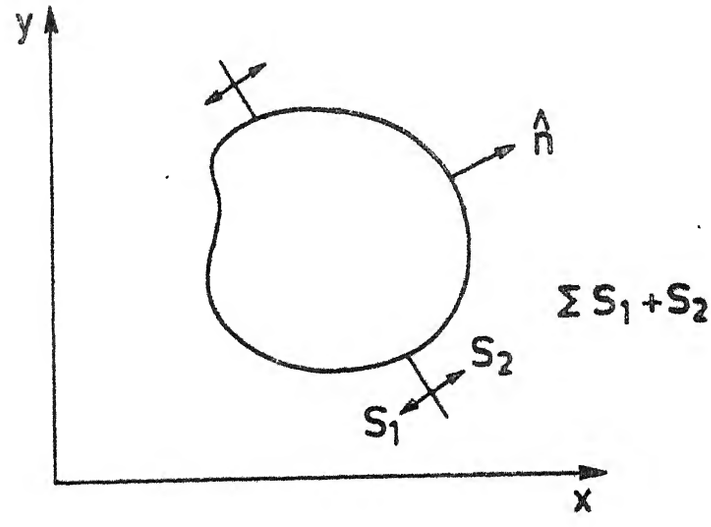

Fig. 2.2 Two dimensional body experiencing different boundary conditions.

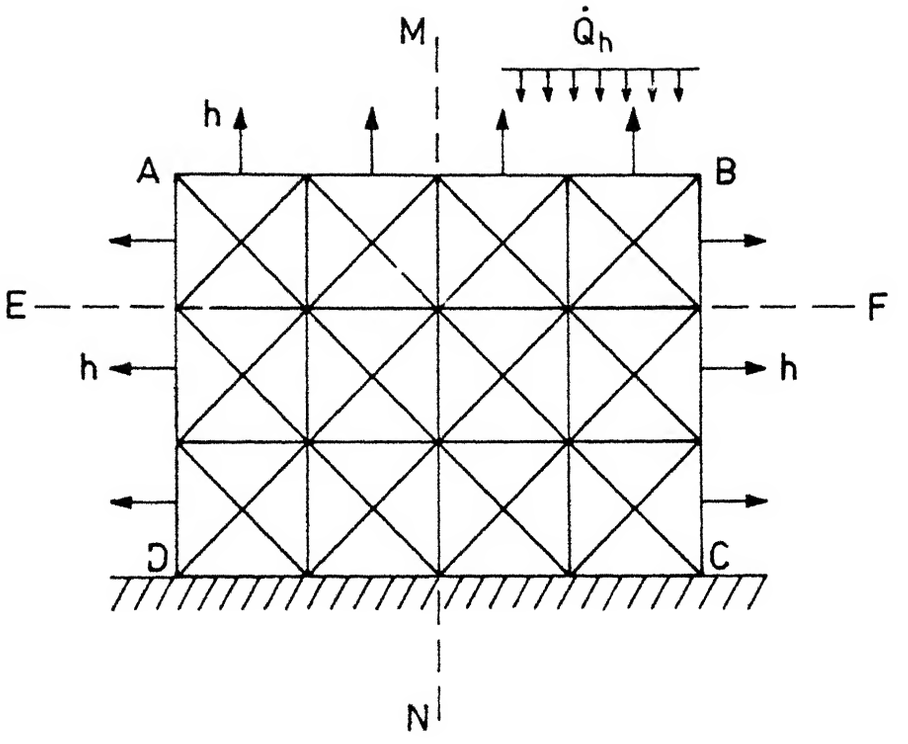

Fig. 2.3 Finite element discretization of the workpiece with boundary conditions.

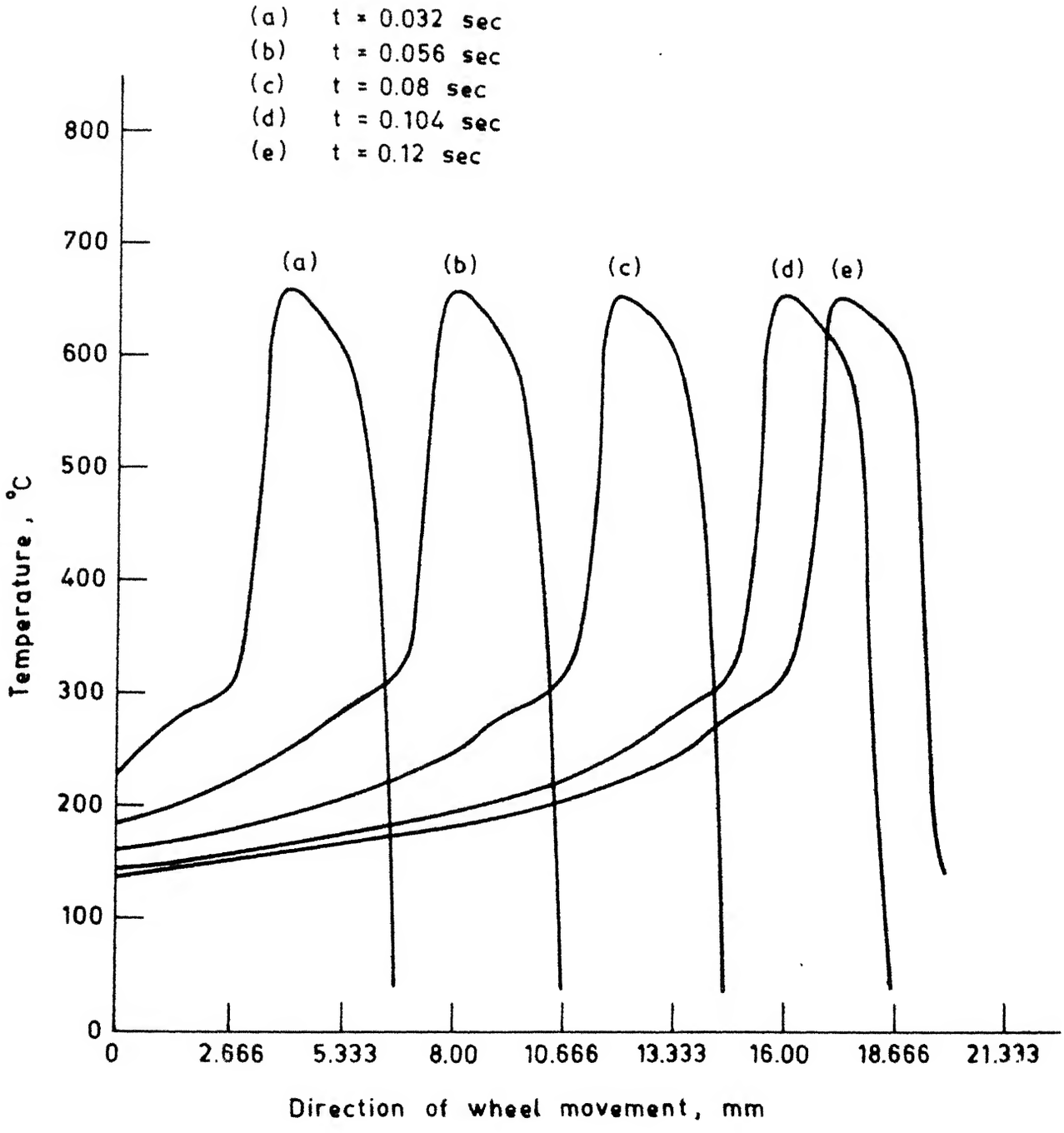

Fig. 2.4 Surface temperature history (set no. 2).

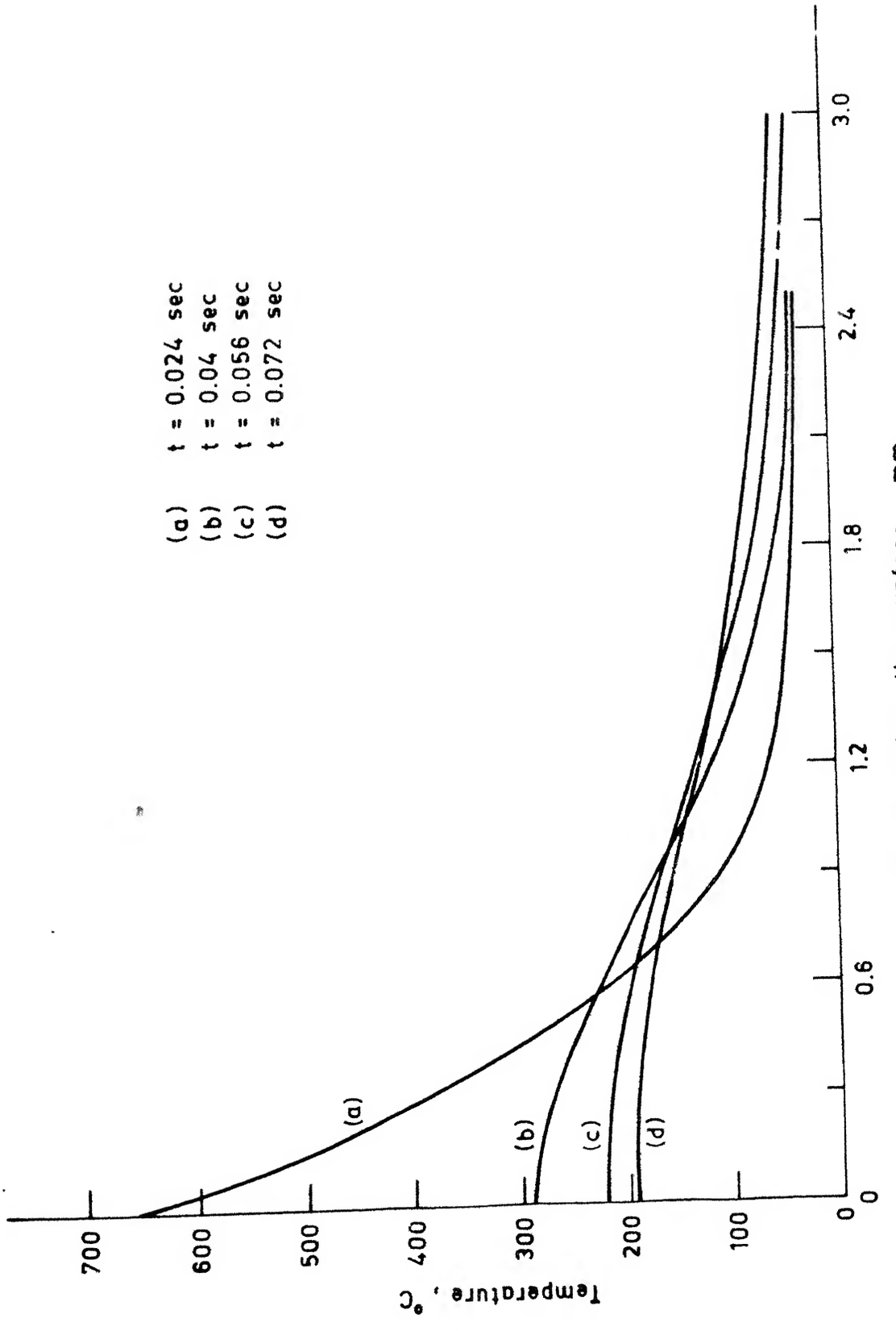

Fig. 2.5 Variation of temperature with depth from the surface at different wheel positions (set no. 2).

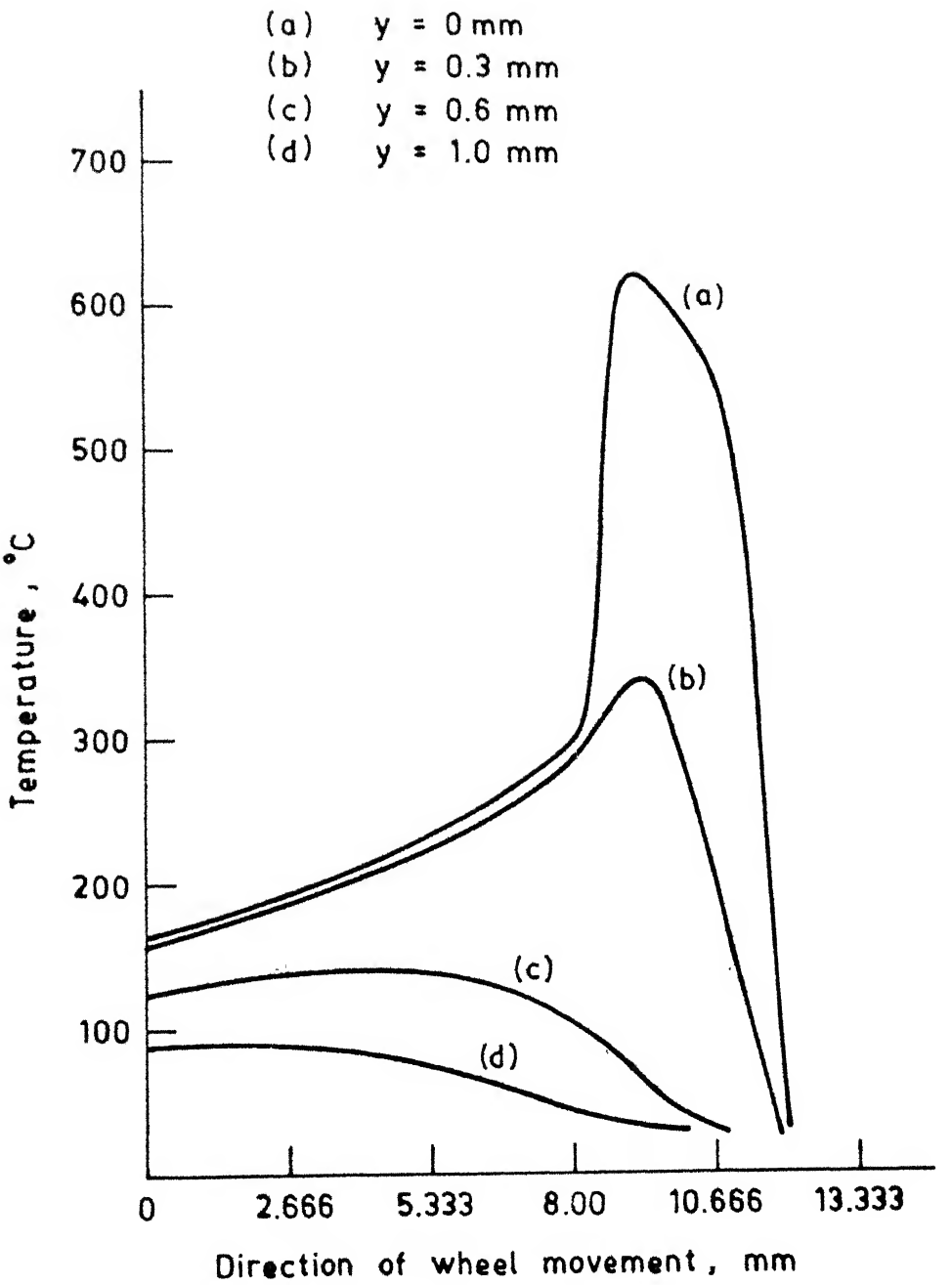

Fig. 2.6 Temperature distribution at various depths from the surface (set no. 3).

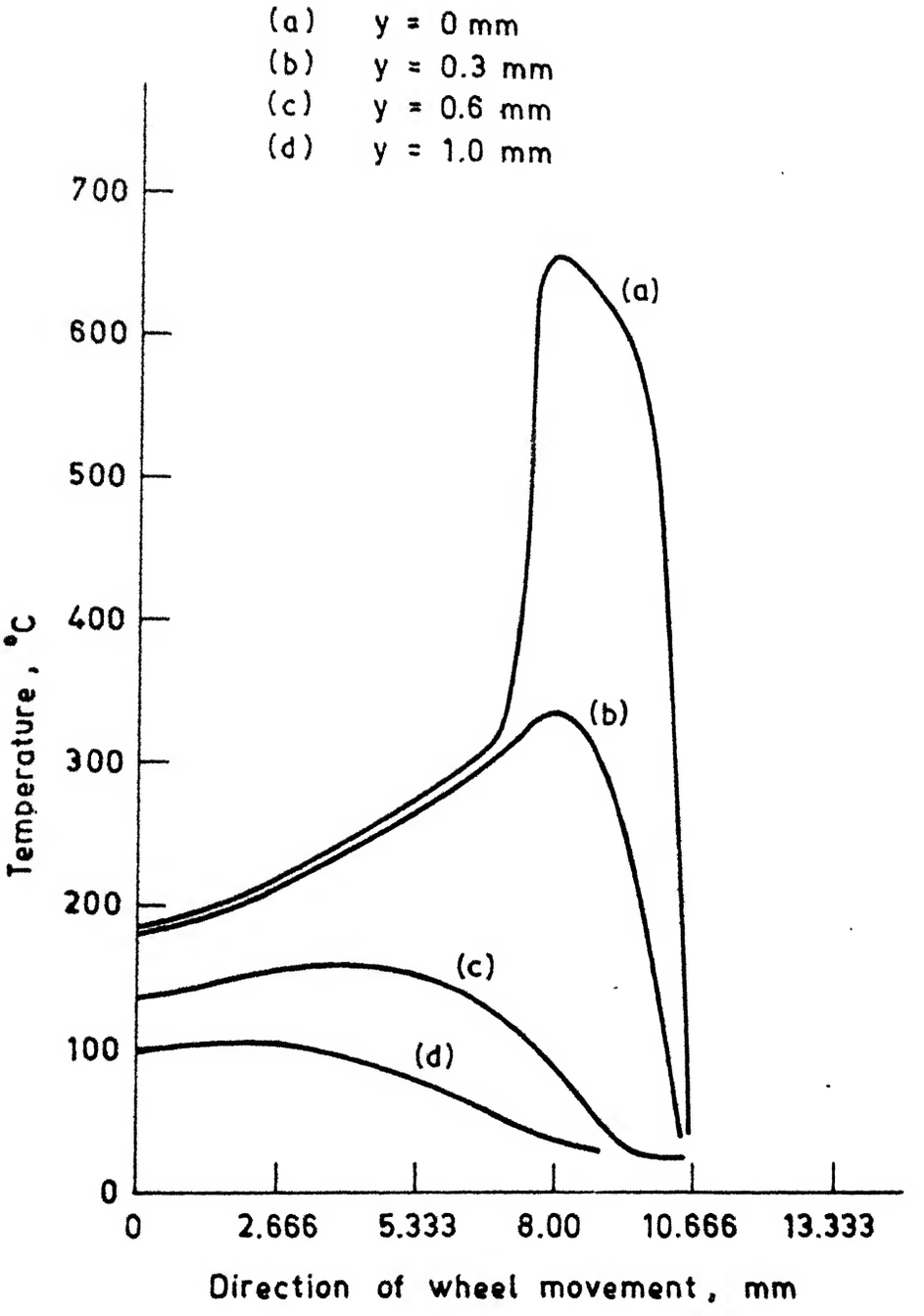

Fig. 2.7 Temperature distribution at various depths from the surface (set no. 2).

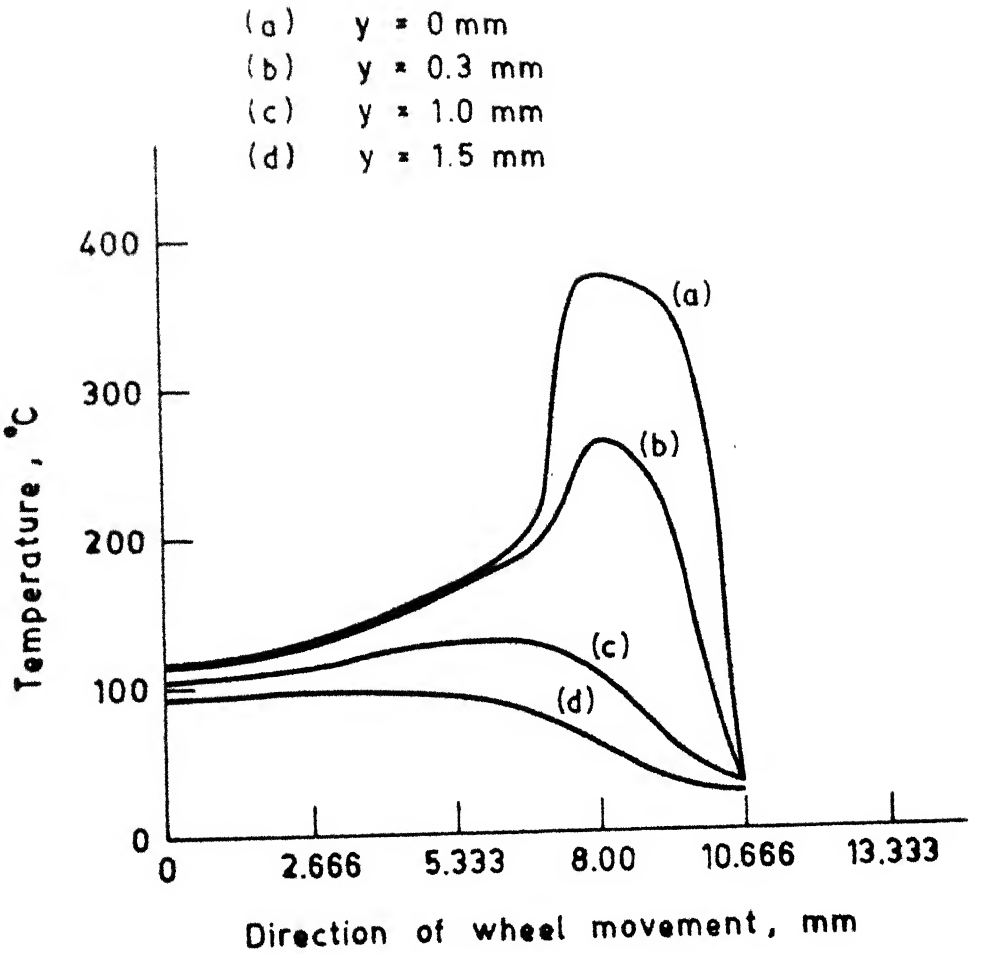

Fig. 2.8 Temperature distribution at various depths from the surface. (set no. 1).

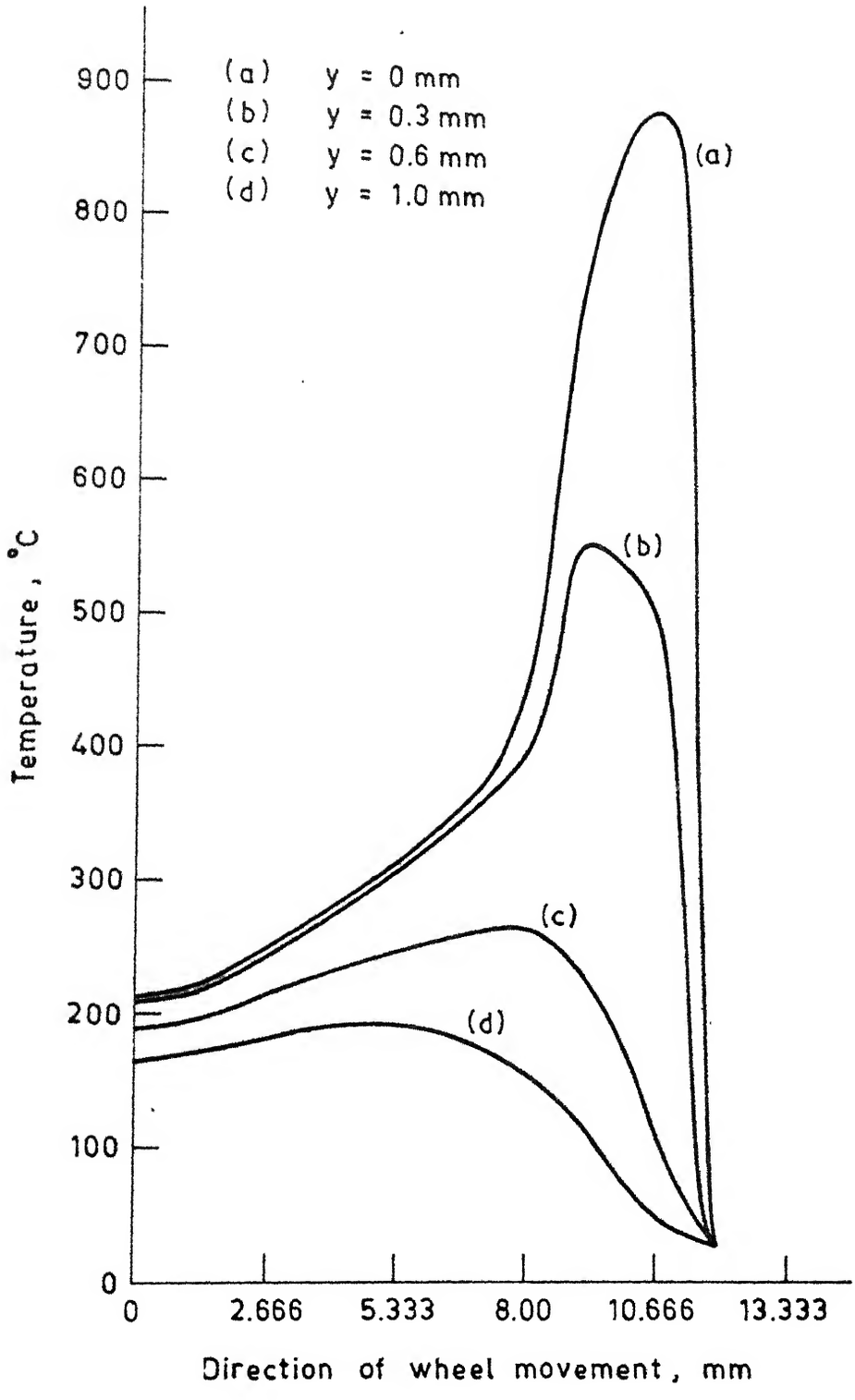

Fig. 2.9 Temperature distribution at various depths from the surface (set no. 4).

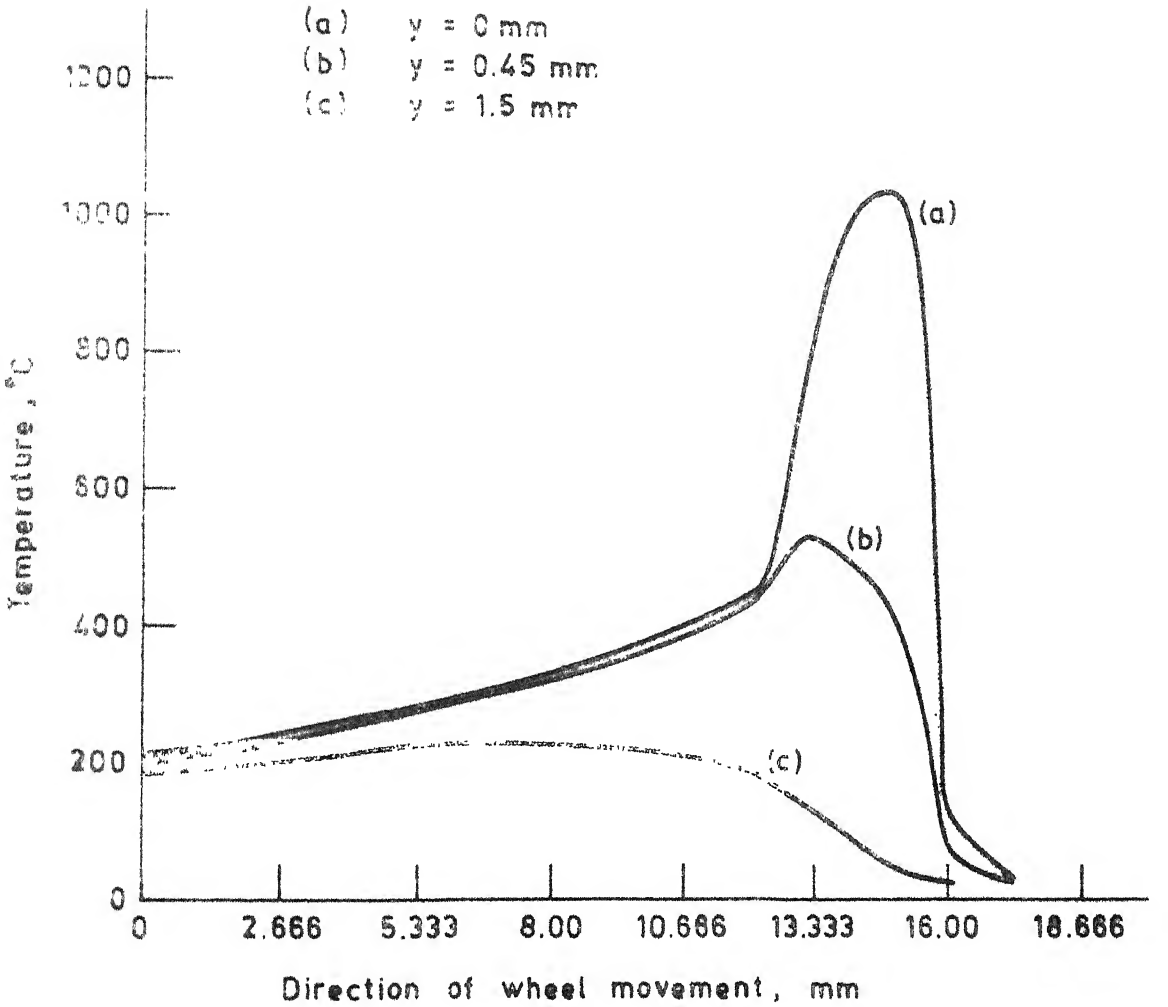

Fig. 2.10 Temperature distribution at various depths from the surface (set no. 7).

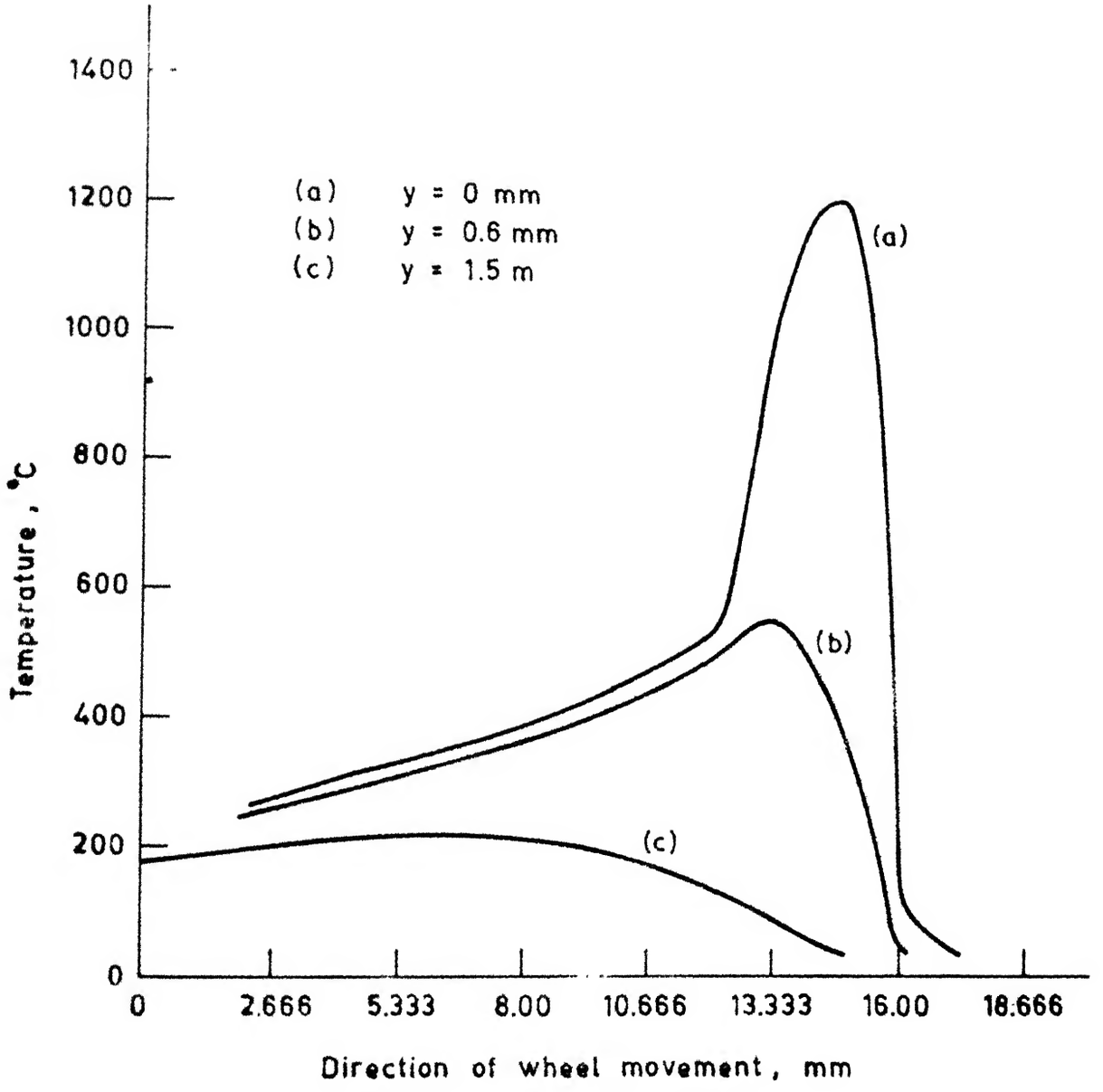

Fig. 2.11 Temperature distribution at various depths from the surface (set no. 8).

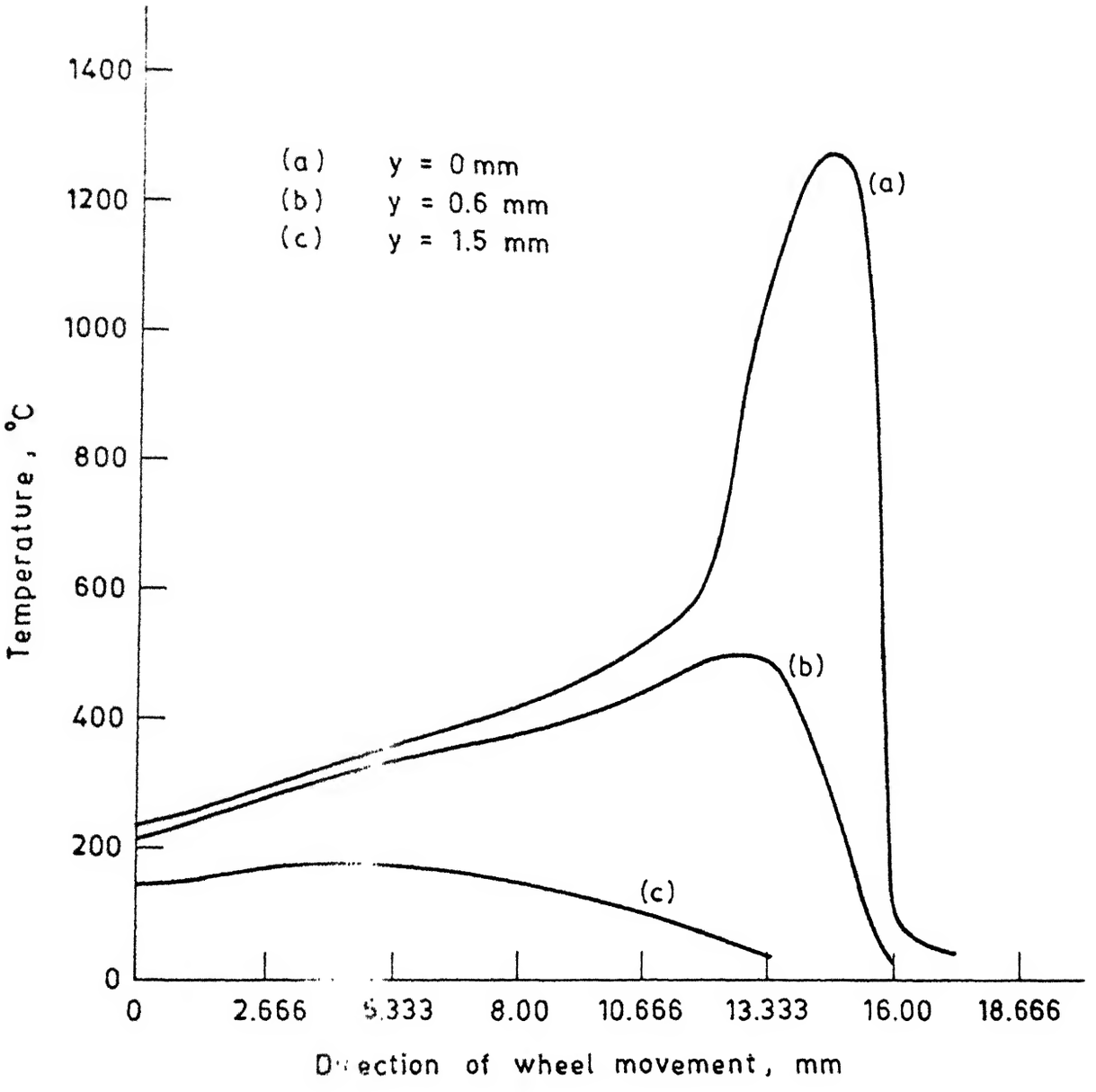

Fig. 2.12 Temperature distribution at various depths from the surface (set no. 9).

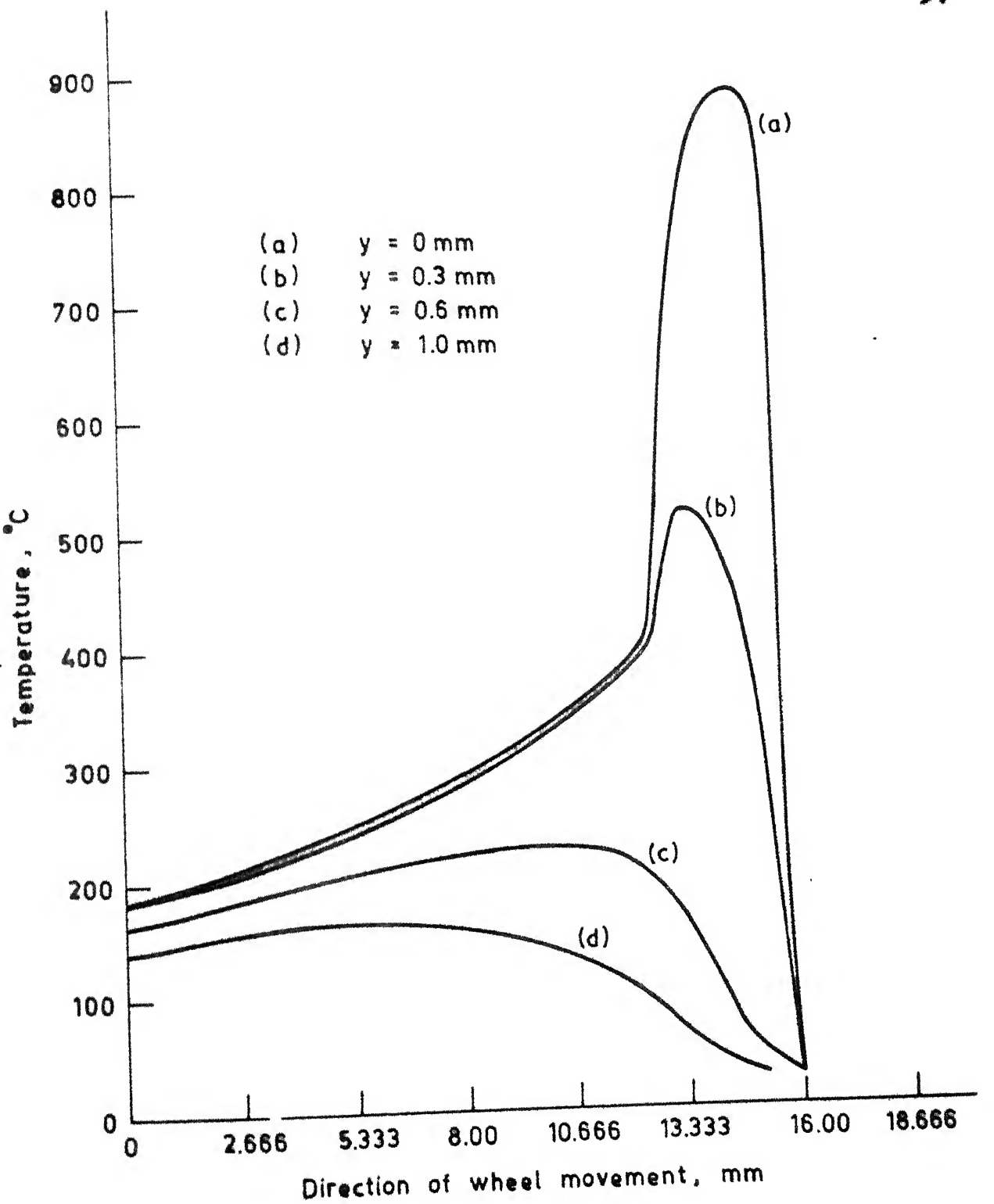

Fig. 2.13 Temperature distribution at various depths from the surface (set no. 5).

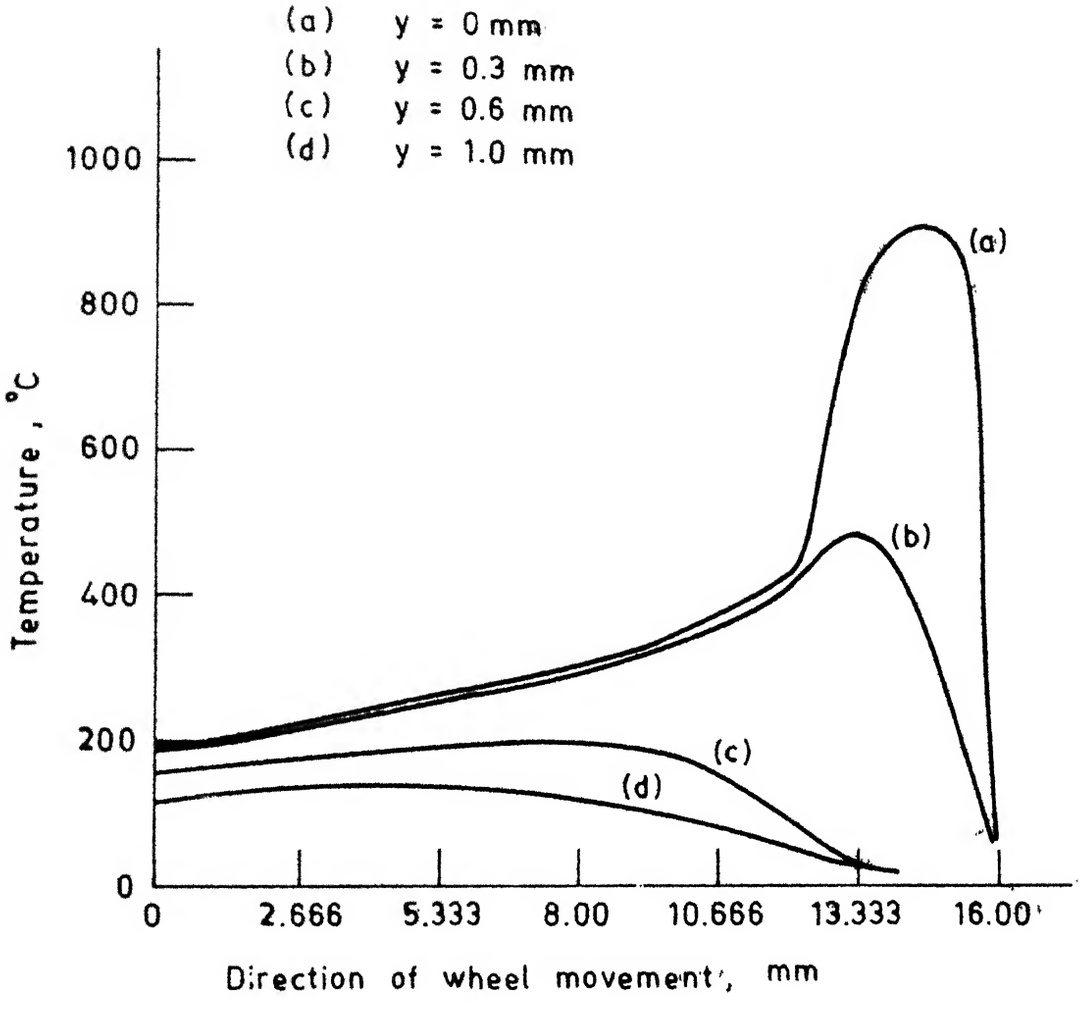

Fig. 2.14 Temperature distribution at various depths from the surface (set no. 6).

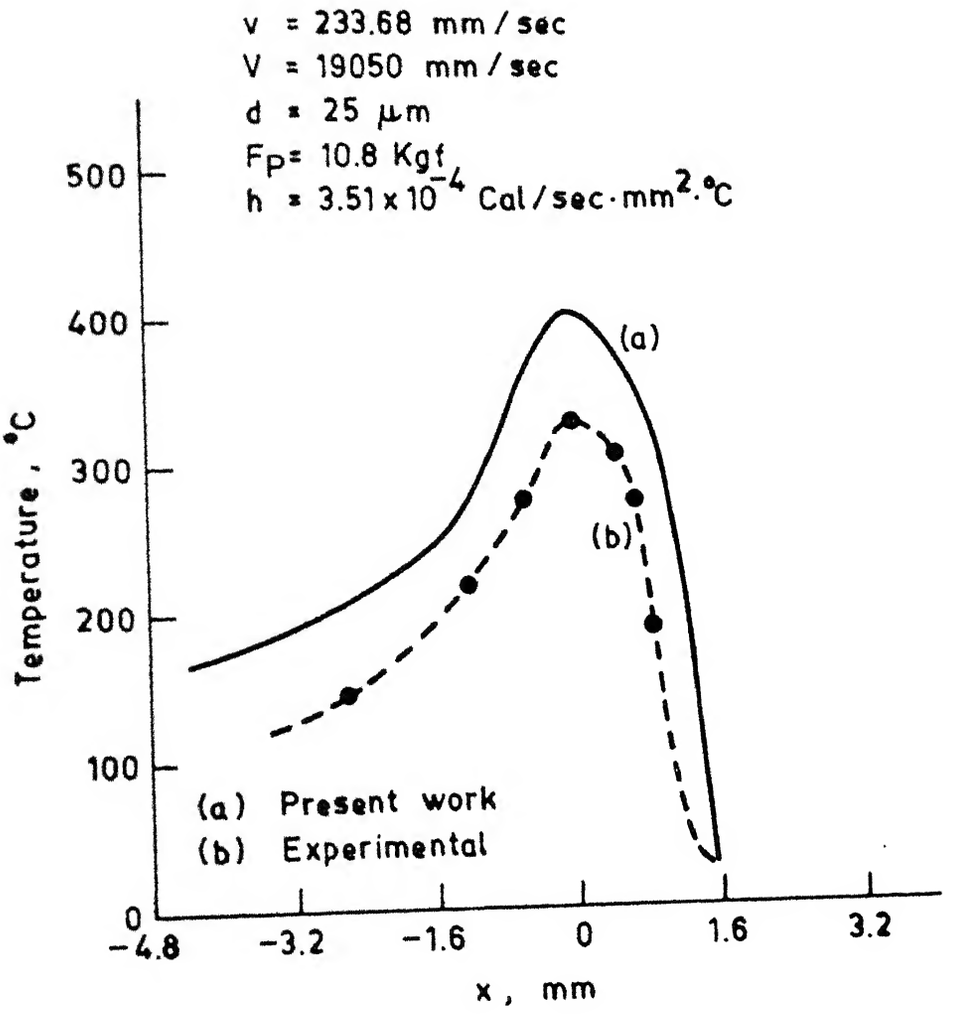

Fig. 2.15 Comparision with experimental data.

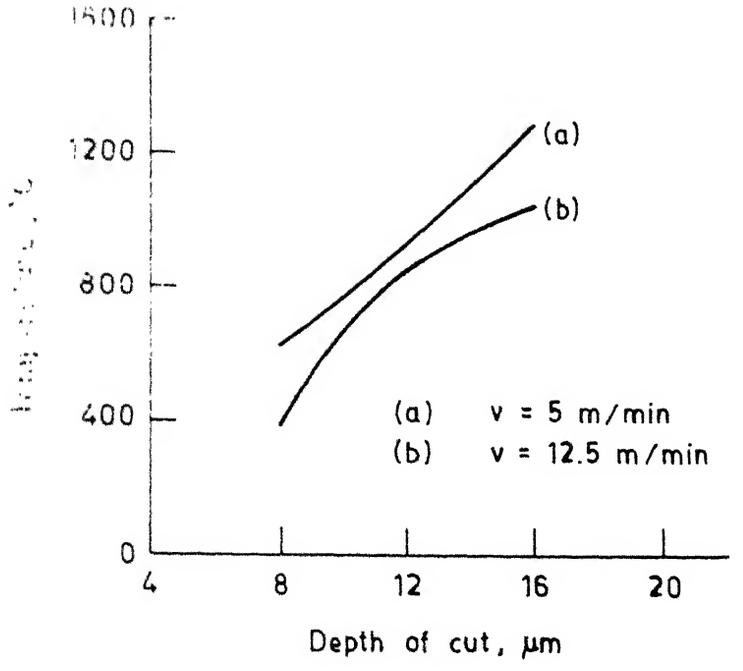

Maximum

Fig. 2.16 Effect of depth of cut on surface temperature.

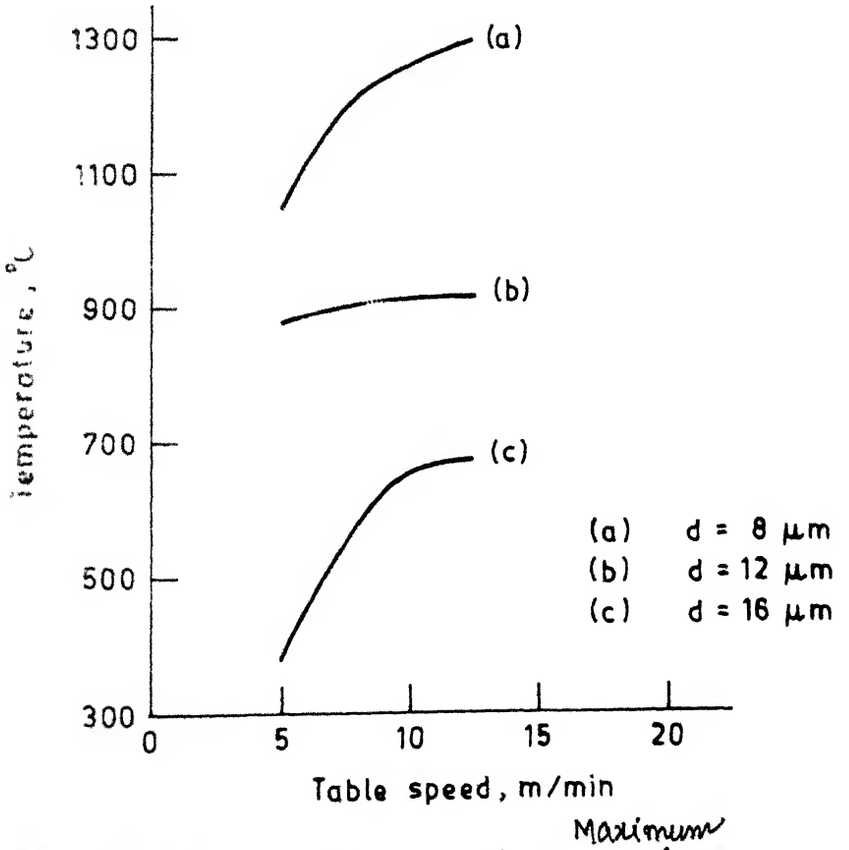

Maximum

Fig. 2.17 Effect of table speed on surface temperature.

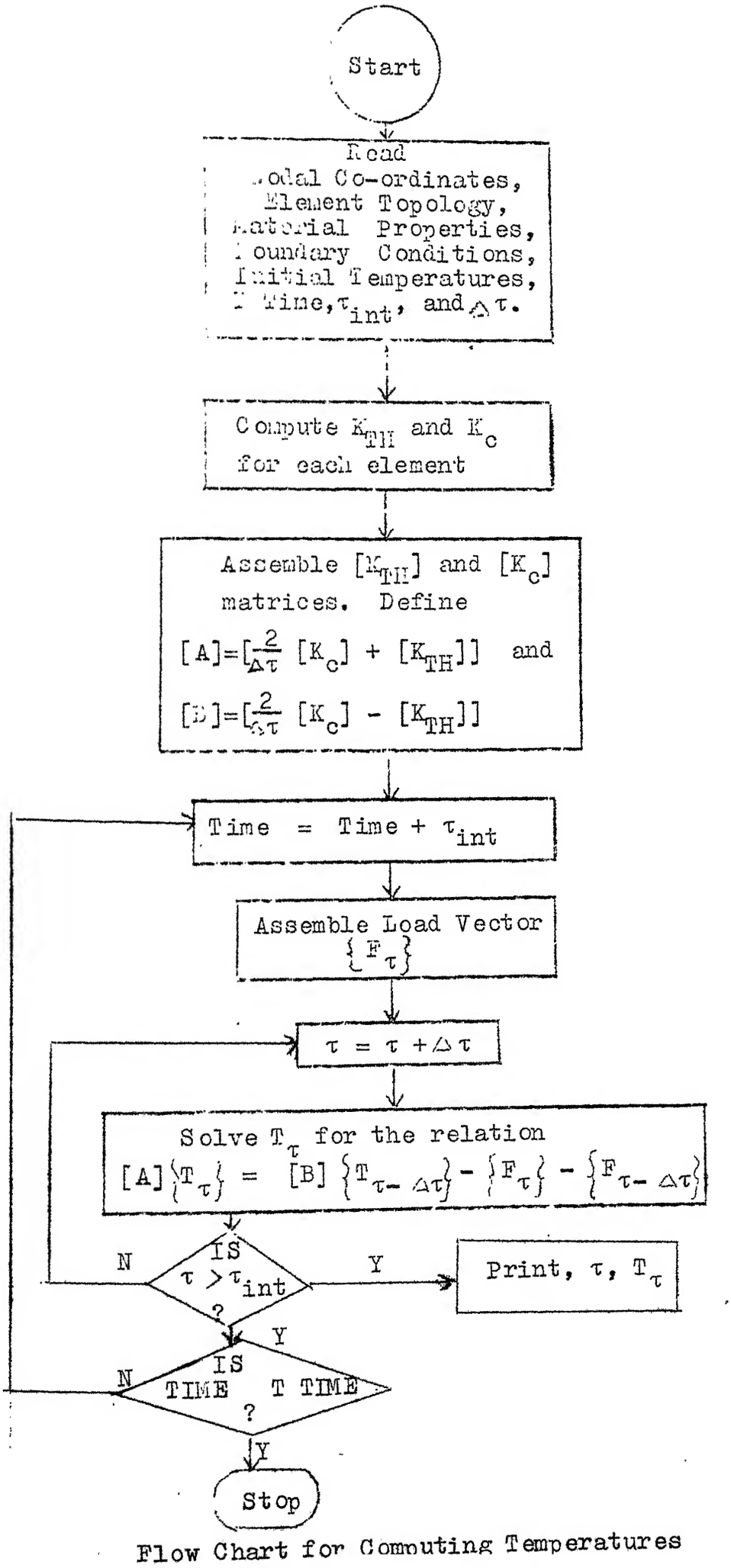

Flow Chart for Computing Temperatures

TABLE 2.1A : INPUT DATA FOR CALCULATING TEMPERATURES. COMPARISON WITH SAUER EXPERIMENTAL RESULTS [8]

S.No.	Wheel speed V (mm/sec)	Table speed v (mm/sec)	Depth of cut d (mm)	Convective coefficient h(cal/mm^2-sec-^{o}C)	Tangential force F_p(gmf)	Temperature ^{o}C	Temperature (Present work) ^{o}C
1	19558	152.4	0.0267	Dry grinding	6078.2	470	540.8
2	19050	241.3	0.028	Dry grinding	9933.84	436.6	550.0
3	19050	307.4	0.02515	2.2464×10^{-3}	12020.4	317.78	460.0
4	19050	233.68	0.0249	3.5108×10^{-4}	10795.68	326.11	385.5
5	19050	233.68	0.026	4.914×10^{-4}	10296.72	386	440.0

TABLE 2.1B : INPUT DATA FOR CALCULATING TEMPERATURES AND STRESSES Ref. [21]

Material : M.S. (60 R_B) Specific Gravity: 0.00779 g/mm^3
Wheel : A46-I5-V10 Young's Modulus : Fig. 3.9
Thermal Conductivity : 0.0146 cal/mm-sec-^oc Poisson Ratio : Fig. 3.9
Specific heat : 0.128 cal/gm-^oc Dry Grinding

S.No.	Wheel speed V(mm/sec)	Table speed v (mm/sec)	Depth of cut d (mm)	Contact length l_c (mm)	Tangential force (gmf)	Average heat flux cal/mm^2-sec
1	23562	83.33	0.008	1.55	4000	11.43
2	23562	166.66	0.008	1.55	10000	28.68
3	23562	208.33	0.008	1.55	10500	30.17
4	23562	83.33	0.012	1.9	9500	22.15
5	23562	125.00	0.012	1.9	11500	27.44
6	23562	208.33	0.012	1.9	16000	37.5
7	23562	83.33	0.016	2.2	11250	22.65
8	23562	125.00	0.016	2.2	16000	32.3
9	23562	208.33	0.016	2.2	22500	45.55

CHAPTER III

RESIDUAL STRESS ANALYSIS

3.1 INTRODUCTION

As explained earlier, the residual stresses are mainly due to non-uniform temperature distribution in the workpiece developed during grinding. These stresses, which are tensile in nature, may sometimes surpass the yield limit of the workpiece material, resulting in crack formation. These cracks, however small they may be initially, grow under the operating conditions of the workpiece, leading to its premature failure.

Much of the work done in the past were to estimate the residual stresses experimentally using bending-deflection technique or X-ray diffraction. With the development of numerical techniques like Finite Element Method, attempts have been made to predict these stresses theoretically.

Thermal stresses in an elastic-plastic continuum can be obtained from the method suggested by Zienkiwicz et al. [18]. This method has been applied to evaluate residual stresses in grinding by Mishra et al. [17]. In the present work, the temperature dependence of Youngs Modulus and Poisson ratio [22] are considered and the work has been extended to study the effects of depth of cut, table speed, and cooling fluid on the residual stresses.

3.2 ANALYSIS

Most applications of Finite Element Method to Solid Mechanics problems rely on the use of variational principle to derive the necessary element properties and final equations. A displacement field within each element is assumed in order to invoke the potential energy principle. This is called displacement method or compatibility method in Finite Element Analysis.

Consider an elastic body of a given shape, deformed by the action of body forces and surface tractions as shown in Fig. 3.1.

The potential energy of such a body is defined as the energy of deformation of the body minus in work done on the body by the external forces, and is given by

$$\pi(u,v) = \frac{1}{2} \iint_A [[\bar{\delta}][B]^T[C][B]\{\bar{\delta}\} - 2[\bar{\delta}][B]^T[C]\{\varepsilon_o^*\}]t\,dA$$

$$- \iint_A [F^*]\{\bar{\delta}\}\,t\,dA - \int_{C_1} [T^*]\{\bar{\delta}\}\,dS \,, \tag{3.1}$$

where

t = thickness of the body

$\{\varepsilon_o^*\}$ = coloumn matrix of initial strains, which is due to non-uniform temperature distribution

$\{ = \begin{Bmatrix} u(x,y) \\ v(x,y) \end{Bmatrix}$ = coloumn matrix of the components of displacement field measured from some datum.

$[$ = matrix relating strains and displacements (Ref: Appendix)

$[$ = material stiffness matrix (Ref: Appendix)

$^{*}]$ = body force components

$^{*}]$ = boundary traction components acting on position C of the boundary (Fig. 3.1).

The discrete values of the displacement components assumed within each element having r nodes and are related their nodal values by r interpolating functions $N_i(x,y)$ as

$$\{ \quad = \begin{Bmatrix} u(x,y) \\ \\ v(x,y) \end{Bmatrix}^{(e)} = \begin{Bmatrix} \sum_{i=1}^{r} N_i(x,y)\, u_i \\ \\ \sum_{i=1}^{r} N_i(x,y)\, v_i \end{Bmatrix} = \begin{Bmatrix} [N] \{u\} \\ \\ [N] \{v\} \end{Bmatrix}, \tag{3.2}$$

Substituting equation (3.2) in equation (3.1), the potential energy for an element is

$$\begin{aligned} \pi^{(e)} = \tfrac{1}{2} \iint_{A^{(e)}} & [\,[\bar{\delta}]^{(e)} [B]^{T(e)} [C]^{(e)} [B]^{(e)} \{\bar{\delta}\}^{(e)} \\ & - 2[\bar{\delta}]^{(e)} [B]^{T(e)} [C]^{(e)} \{\varepsilon_o^{*}\}^{(e)}\,] t^{(e)} dA^{(e)} \\ & - \iint_{A^{(e)}} [F^{*}]^{(e)} \{\bar{\delta}\}^{(e)} t^{(e)} dA^{(e)} - \int_{C_1^{(e)}} [T^{*}]^{(e)} \{\bar{\delta}\}^{(e)}\, dA^{(e)}, \end{aligned} \tag{3.3}$$

The potential energy of the discrete system assumes its minimum value when the first variation of the functional vanishes. At any node q, we have

$$\begin{Bmatrix} \frac{\partial \pi^{(e)}}{\partial u_q} \\ \frac{\partial \pi^{(e)}}{\partial v_q} \end{Bmatrix} = \{0\} = \iint_{A^{(e)}} [B]_q^T [C]_q^{(e)} [B]_q^{(e)} \{\bar{\delta}\}_q^{(e)} t^{(e)} dA^{(e)}$$

$$- \iint_{A^{(e)}} [B]_q^T [C]_q^{(e)} \{\varepsilon_o^*\}^{(e)} t^{(e)} dA^{(e)}$$

$$- \iint_{A^{(e)}} N_q \{F^*\}_q^{(e)} t^{(e)} dA^{(e)}$$

$$- \int_{C_1 q^{(e)}} N_q \{T^*\}_q^{(e)} dS_q^{(e)}, \qquad (3.4)$$

where

$\{\bar{\delta}\}_q = \begin{Bmatrix} u_q \\ v_q \end{Bmatrix}$ = coloumn vector of the displacement components at node q.

Equation (3.4) is the Force-Displacement relation for the node q. In matrix notation, it can be expressed as

$$\underset{2x2}{[K]_q} \underset{2x1}{\{\bar{\delta}\}_q} = \underset{2x1}{\{F_o\}_q} + \underset{2x1}{\{F_B\}_q} + \underset{2x1}{\{F_T\}_q} + \underset{2x1}{\{F\}_q}, \qquad (3.5)$$

where

$[K]_q$ = stiffness matrix at node q

$\{F_o\}_q = \iint_{A^{(e)}} [B]_q^{T(e)}\,{}^{2\times3}\,[C]^{(e)}\,{}^{3\times3}\,\{\varepsilon_o^*\}^{(e)}\,{}^{3\times1}\,t^{(e)}\,dA^{(e)}$ = initial force vector at node q

$\{F_B\}_q = \iint_{A^{(e)}} N_q(x,y)\,\{F_q\}^{(e)}\,{}^{2\times1}\,t^{(e)}\,dA^{(e)}$ = nodal body force vector

$\{F_T\}_q = \iint_{C_1^{(e)}} N_q(x,y)\,\{T^*\}_q^{(e)}\,dS_q^{(e)}$ = nodal force vector due to surface loading

$\{F\}_q$ = external load vector at node q.

Equation (3.5) is calculated for all the nodes of an element, and than assembled for all the elements to form global stiffness matrix and load vector. The element chosen here is the same triangular element used in the calculation of the temperatures and the element stiffness matrix is given in Appendix. The final equation takes the form

$$[K_D]\{\delta\} = \{F_L\} \quad , \tag{3.6}$$

where

$[K_D]$ = total stiffness matrix

$\{\delta\}$ = displacement vector

$\{F_L\}$ = load vector.

The strains due to temperature rise in the workpiece can be written, in case of plane strain as

$$\{\varepsilon_o^*\} = \begin{Bmatrix} \varepsilon_{xo} \\ \varepsilon_{yo} \\ \gamma_{xyo} \end{Bmatrix} , \qquad (3.7)$$

where ε_{xo} and ε_{yo} are the normal strains and γ_{xyo} is the shear strain. For an isotropic material, the strain vector in an element subjected to a temperature rise T is

$$\{\varepsilon_o^*\} = (1+\nu) \begin{Bmatrix} \alpha \Delta T \\ \alpha \Delta T \\ o \end{Bmatrix} , \qquad (3.8)$$

where

ν = poisson ratio

α = coefficient of linear expansion

ΔT = temperature increment.

The equivalent loads corresponding to the strain vector are given by

$$\{F_{eq}\} = \iint_{A^{(e)}} [B]^T [C] \{ \varepsilon_o^* \} \, dA^{(e)} , \qquad (3.9)$$

The thermal stress at any point in an element, for elastic behaviour of material is obtained from the relation

$$\{S\} = [C] [B] \{\delta\}^{(e)} - [C] \{\varepsilon_o^*\} , \qquad (3.10)$$

where

$$\{S\} = \begin{Bmatrix} S_x \\ S_y \\ S_{xy} \end{Bmatrix}$$

$\{\delta\}^{(e)}$ = element displacements.

In the present work, Von-mises yield criterion is assumed, and the material is assumed to be elastic perfectly plastic. For a plane strain case, yield occurs when

$$Y(T) \leq \bar{S} , \qquad (3.11)$$

where

$Y(T)$ = yield stress at temperature T

$\bar{S}$ = effective stress $= \sqrt{\frac{1}{2}\{ S_x^2+S_y^2-S_xS_y+3S_{xy}^2 \}}$

S_x, S_y = longitudinal and transverse stresses,

S_{xy} = shear stress.

The check in equation (3.11) is carried out for all the elements. In the elements where yield has taken place, the excess stresses beyond is calculated and redistributed in the following manner :

(1) Calculate $r = \frac{Y(T)}{\bar{S}}$.

(2) Calculate excess stress as $(1-r)S_x$, $(1-r)S_y$, $(1-r)S_{xy}$, where S_x, S_y, S_{xy} are the components of stress for elastic behaviour of material.

(3) Calculate the corresponding loads

$$\{F_L\} = -\iint_{A^{(e)}} [B]^T \{S_o\} \, dA^{(e)} , \qquad (3.12)$$

where

$\{S_o\}$ = vector containing excessive stresses.

(4) Solve the elastic problem once again,

(5) Modify the stresses at all points in the continuum by adding the stresses obtained in step (4) to the previous values. This process is continued till the difference between two successive values of stresses reach a minimum.

(6) Proceed for all the incremental thermal loads resulting from the movement of the wheel, in a similar way.

A computer flow chart depiciting the various steps involved in the calculation of residual stresses is given at the end of the chapter.

From the previous chapter, it was found that the temperature gradients exist only in a shallow region below the workpiece surface. The displacements at a depth below this affected zone are negligible compared to those at the surface. The displacements on the plane EF (Fig. 2.3) are therefore, assumed to be zero. Same discretization model is used for both stress and temperature models [Fig. 2.3].

3.3 RESULTS

With the temperatures obtained using the theoretical analysis in the previous chapter, the stresses in the workpiece were calculated. The input parameters are given in Table 2.1B. The results are plotted in Fig. 3.2 - Fig. 3.6. The nature of the curve, and the order of magnitude of the stresses match with the experimental data available [12]. With the increase in table speed, residual stresses increase (Fig. 3.4). And also with the increase in depth of cut, there is considerable increase in the peak value of the residual stress (Fig. 3.3). The effect of the cooling fluid on the peak values of tensile residual stress is plotted in Fig. 3.6. The stress history in the workpiece is shown in Fig.3.2. The variation of transverse residual stresses are shown in Fig. 3.5.

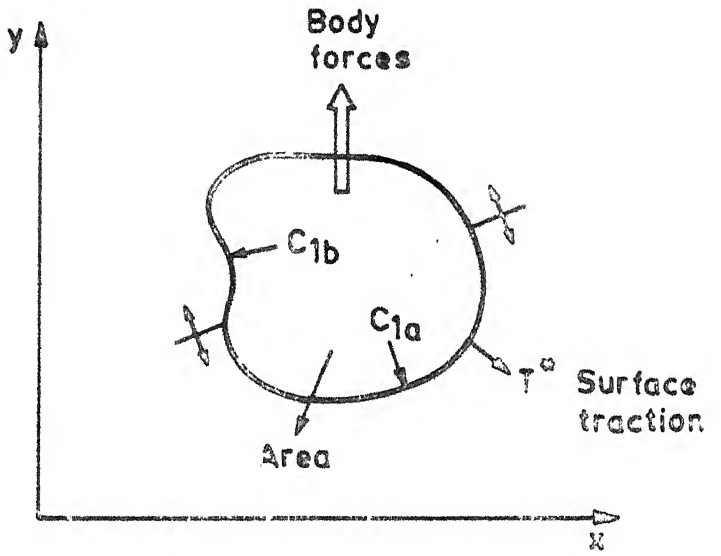

Fig. 3.1 Arbitary two dimensional elastic body experiencing surface tractions and body forces.

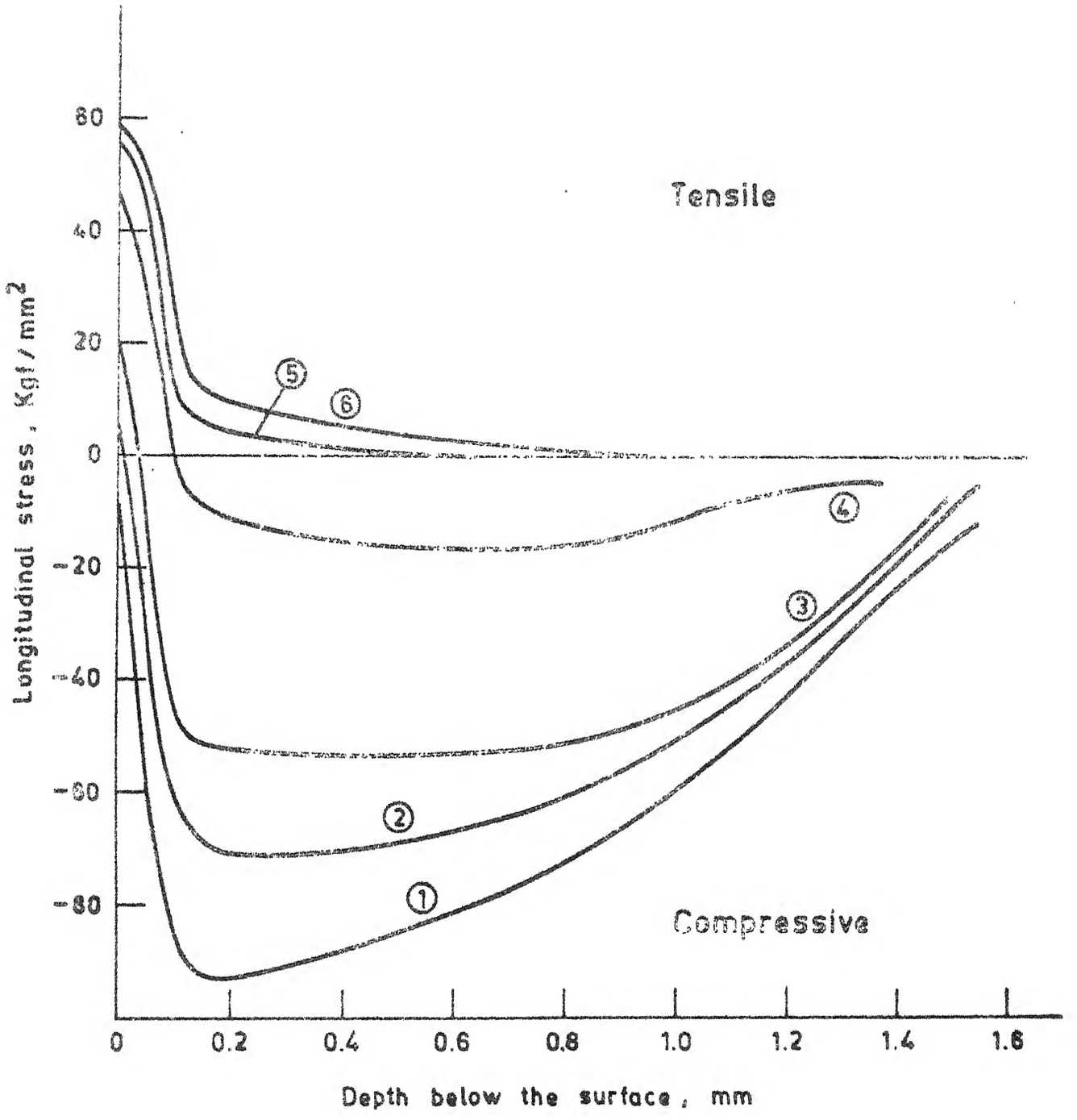

Fig. 3.2 Residual stress - history inside the workpiece (set no. 5) Table 2.1B.

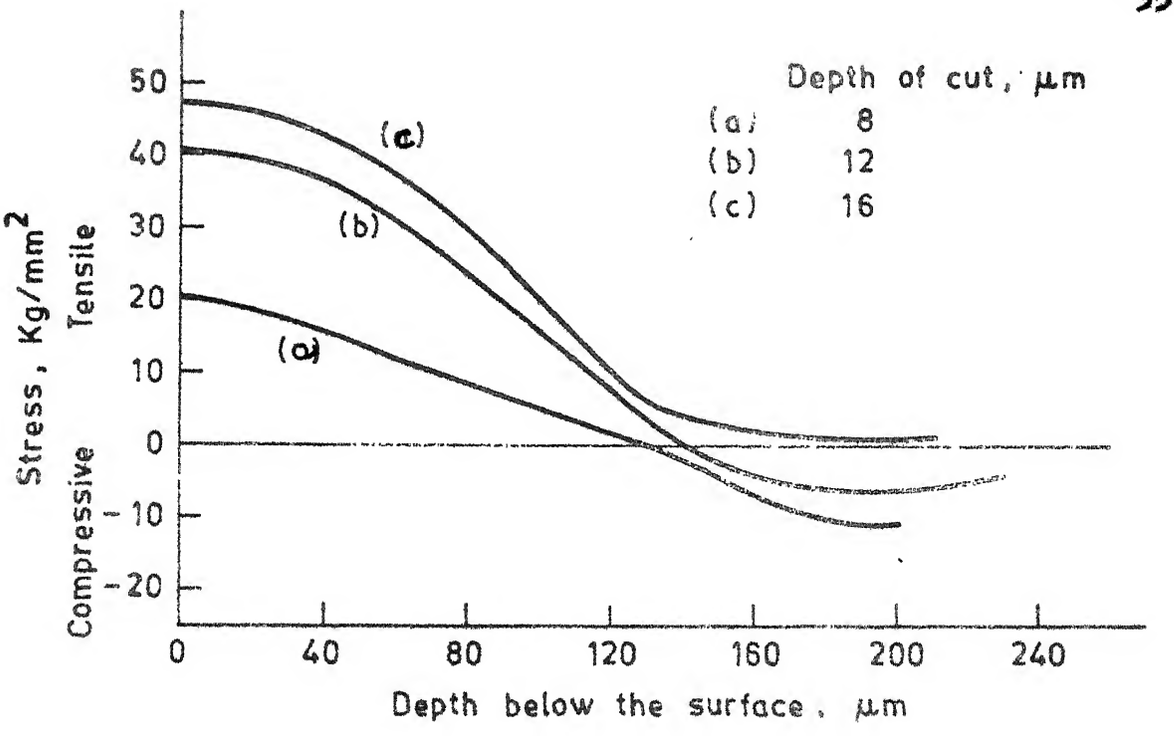

Fig. 3.3 Effect of depth of cut on residual stress distribution (set no. 1,4,7), table 2.1B

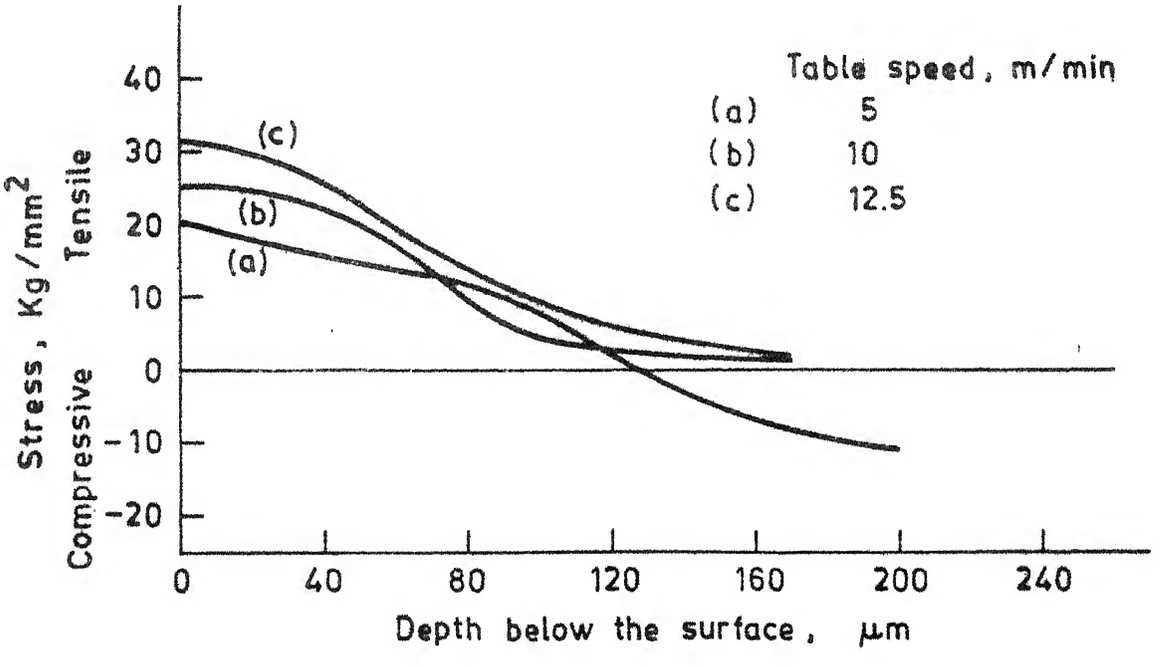

Fig. 3.4 Effect of table speed on residual stress distribution (set no. 1,2,3), table 2.1B

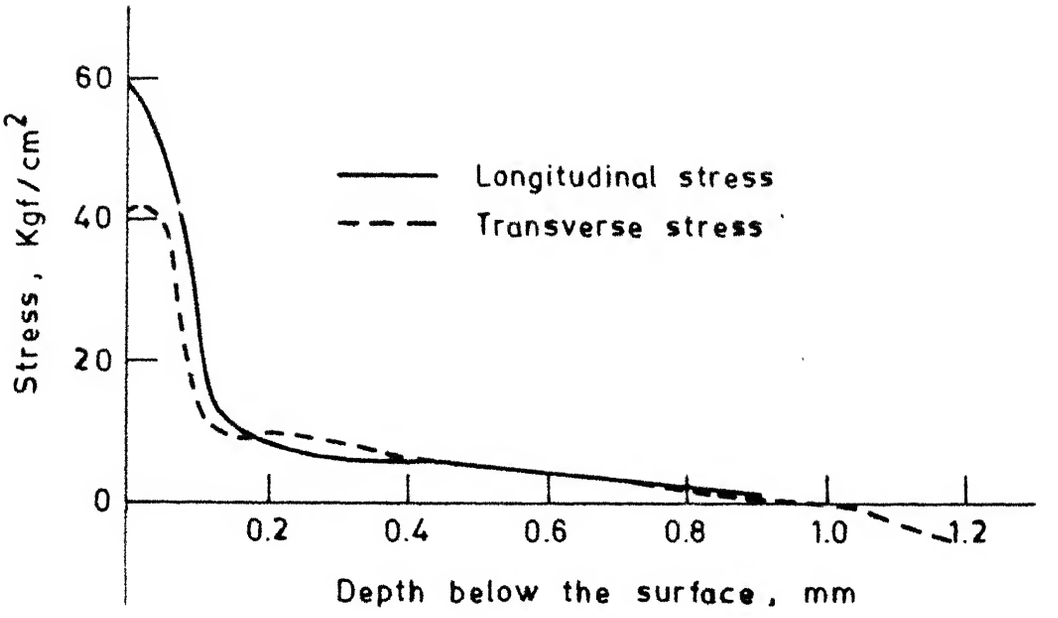

Fig. 3.5 Residual stress distribution (set no. 5).

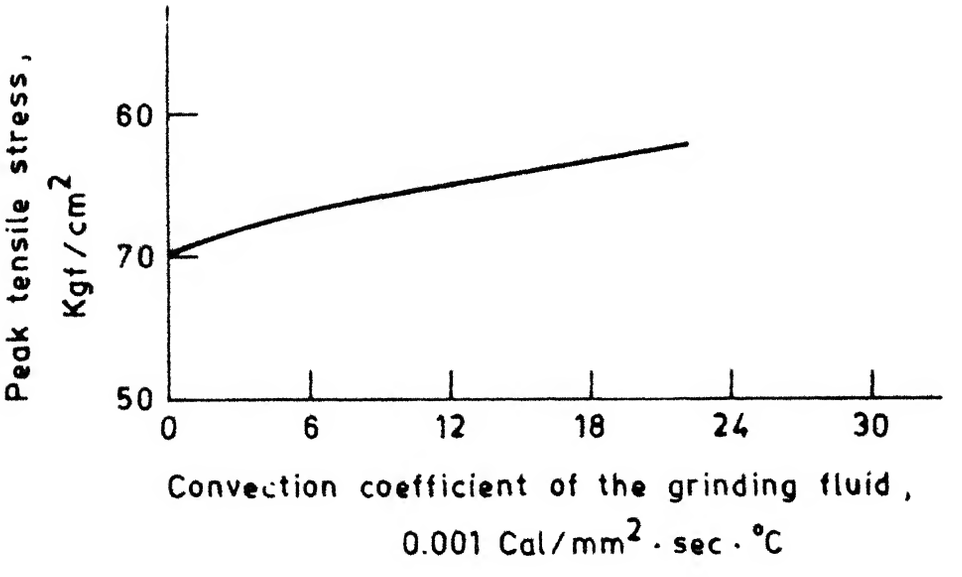

Fig. 3.6 Effect of cooling fluids on peak residual stress.

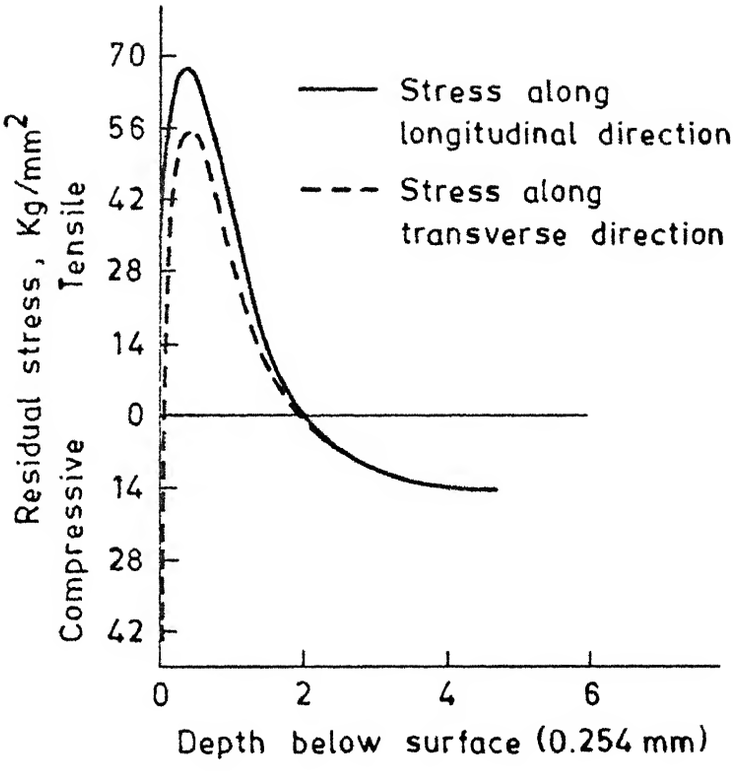

Fig. 3.7 A typical residual stress distribution. After Letner (12)

Wheel speed : 30480 mm/sec
Work speed : 304.8 mm/sec
Cross feed : 1.27 mm/pass
Depth of cut : 0.0508 mm
Grinding fluid : Oil-water emulsion
Work piece material : 52100 steel
Hardness : 59 Rockwell "C"

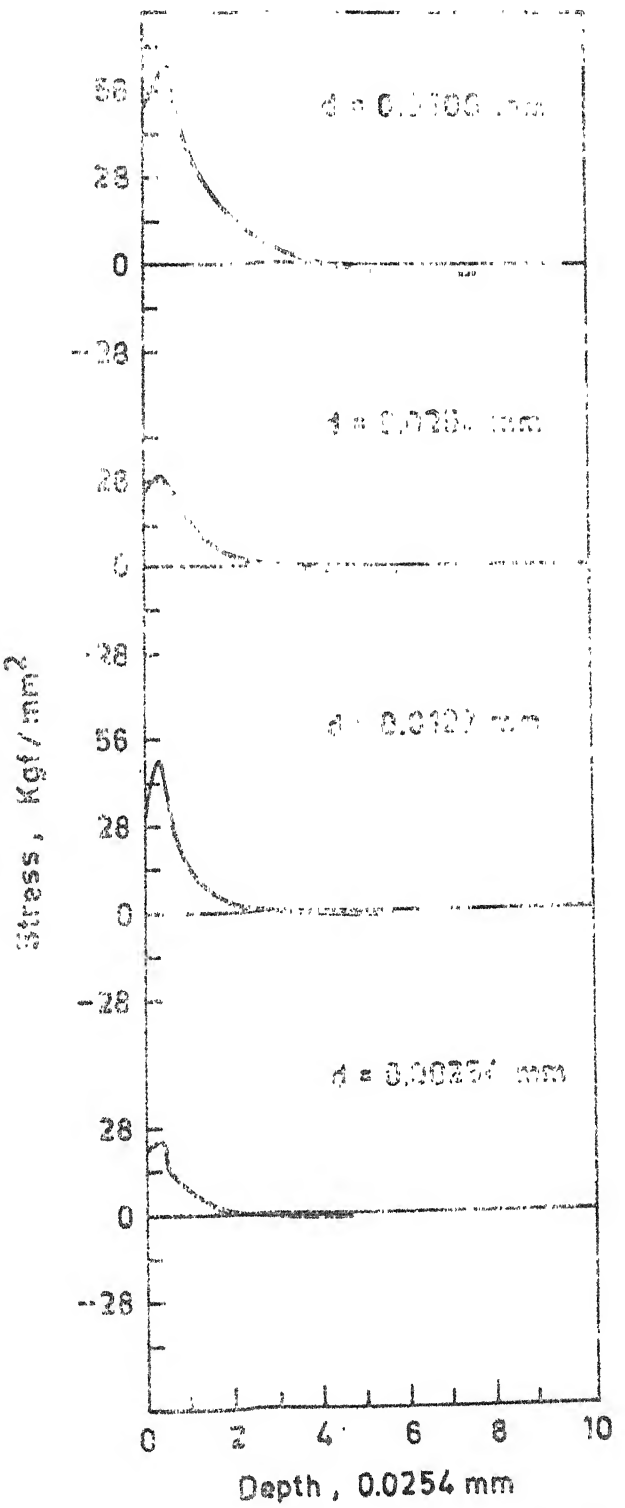

Fig. 3.8 Residual stress distributions resulting from grinding of various depths of cut. (Material : Bearing Steel)
After Letner [19].

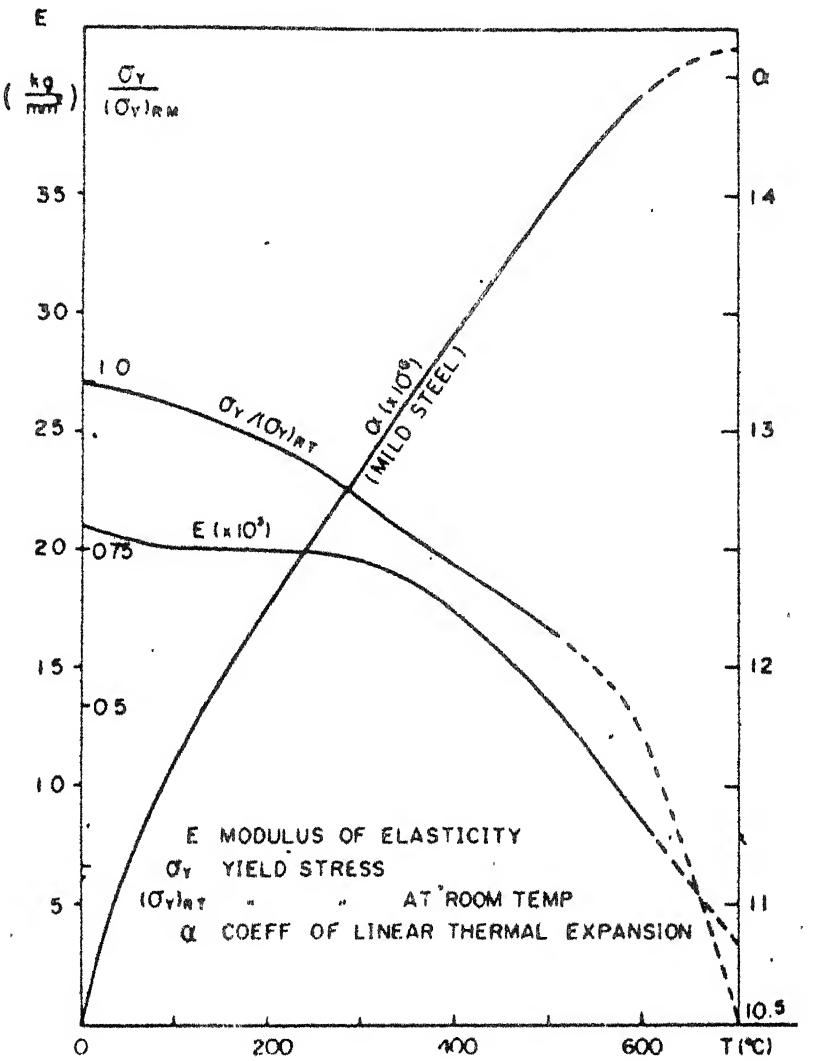

Fig. 3.9 Assumed mechanical properties of mild steel dependent on temperature. [Ref 22]

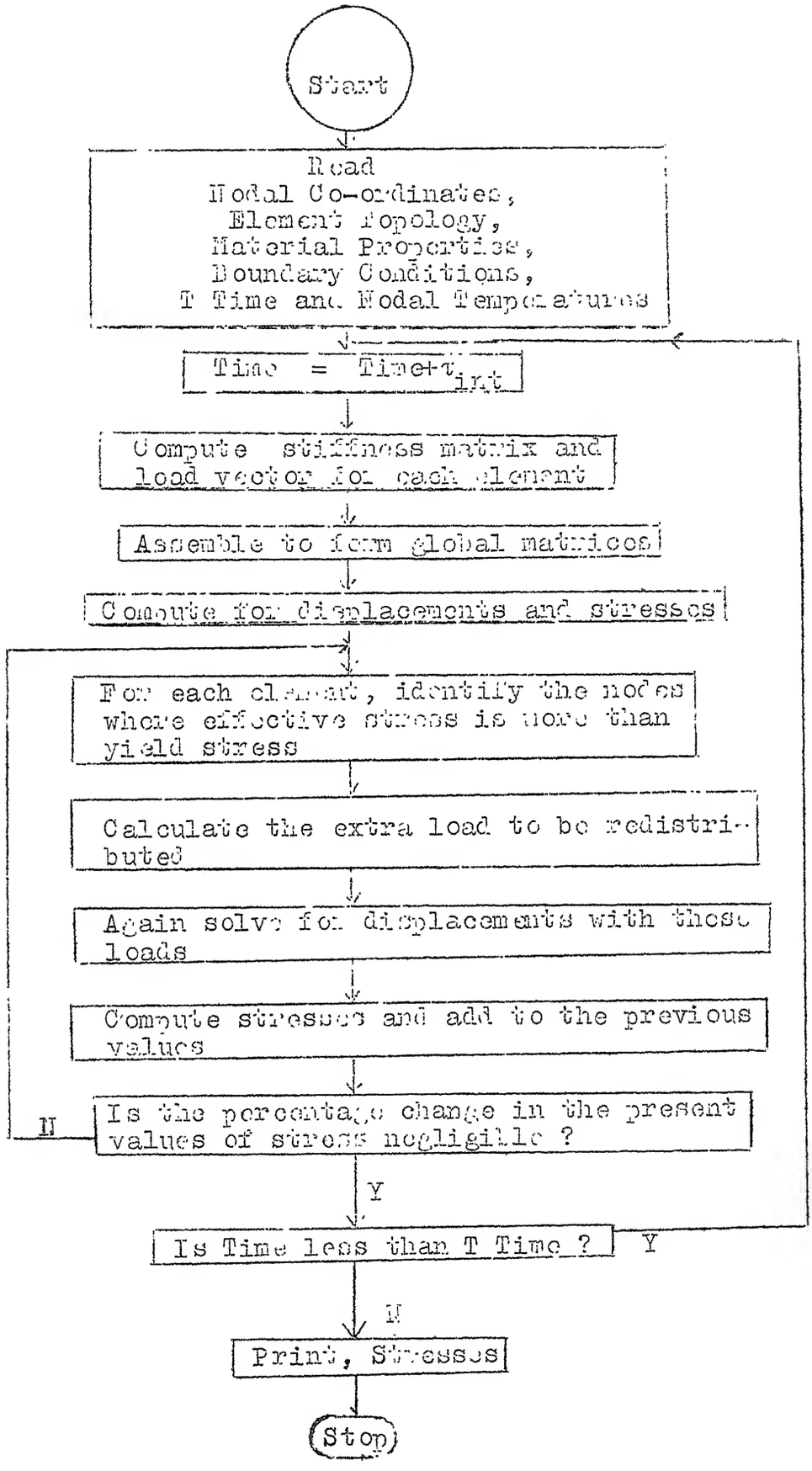

Flow Chart for Computing Residual Stresses.

CHAPTER IV

DISCUSSION OF RESULTS

Finite Element Analysis yields realistic values, provided the material properties and their variation with temperature are exactly known. Finite Element Analysis is based on the concept of discretization, like all other numerical approximations. Despite the fact that a solution is obtained at a finite number of discrete nodal points, the formulation of field variable model inherently provides a solution at all other locations in the body. The main advantage of this method is that complex geometries with difficult boundary conditions can be analysed. But the use of this method is restricted to the availability of large speed computers.

The present model for obtaining temperature and stresses can give realistic values provided the input heat flux $\dot{Q}_F$, and its variation along the contact length l_c is exactly known. From literature [27], it was observed that the assumption that $\dot{Q}_F$ varies uniformly yields good results.

It can be seen from the input data, Table (2.1B), that the forces increase with increase in depth of cut and table speed. The factors that govern the forces are : individual machine settings and their combinations in various forms, dressing techniques, coolants, wheel-workpiece material

combination, rigidity of the machine and so on. From equation (2.2), with increase in force, the heat flux $\dot{Q}_F$ increases thereby increasing the temperatures. This is observed in Figs. 2.4 to 2.14, where the temperatures for different depth of cuts and table speeds are plotted. Increasing depth of cut, increases the temperature but with the increase in table speed, the increase in temperature is marginal. This is because, with increase in table speed, there is a decrease in the fraction of grinding energy entering into the workpiece, which reduces the effect of increase in the tangential force in equation (2.2). Since α is assumed to be a constant, the effect of table speed on temperature is observed to be marginal. At higher table speeds, however, the depth of the affected zone reduces, Figs. 2.6 to 2.8.

Since the stresses are resulting from these temperatures, they also follow a similar variation with depth of cut and table speed. Figs. 3.3 to 3.4 show the plot of the residual stresses as a function of depth below machined surface, for different table speeds and depth of cut. They are tensile in nature at the surface and at lower depths they tend to become compressive in some cases. At higher depths of cut, the peak temperature values obtained are more (Figs.2.8 to 2.10) due to the fact, F_p increases. Also α (equation 2.2) increases with depth of cut. So with the increase in the depth of cut, peak values of stress also increase. From

combination, rigidity of the machine and so on. From equation (2.2), with increase in force, the heat flux $\dot{Q}_F$ increases thereby increasing the temperatures. This is observed in Figs. 2.4 to 2.14, where the temperatures for different depth of cuts and table speeds are plotted. Increasing depth of cut, increases the temperature but with the increase in table speed, the increase in temperature is marginal. This is because, with increase in table speed, there is a decrease in the fraction of grinding energy entering into the workpiece, which reduces the effect of increase in the tangential force in equation (2.2). Since α is assumed to be a constant, the effect of table speed on temperature is observed to be marginal. At higher table speeds, however, the depth of the affected zone reduces, Figs. 2.6 to 2.8.

Since the stresses are resulting from these temperatures, they also follow a similar variation with depth of cut and table speed. Figs. 3.3 to 3.4 show the plot of the residual stresses as a function of depth below machined surface, for different table speeds and depth of cut. They are tensile in nature at the surface and at lower depths they tend to become compressive in some cases. At higher depths of cut, the peak temperature values obtained are more (Figs.2.8 to 2.10) due to the fact, F_p increases. Also α (equation 2.2) increases with depth of cut. So with the increase in the depth of cut, peak values of stress also increase. From

Any discrepency in the values can be attributed to the method by which they are obtained. Finite Element Method is based on discretization of a body into small regions and also, the heat source (wheel) movement is modelled by step wise movements. Better results can be obtained by using finer Finite Element mesh and smaller movements by the wheel. But the computational time will increase. It was also assumed that $\dot{Q}_F$ varies uniformly over the contact length l_c, but in actual grinding process its variation is unknown. As the cut progresses the grain experiences more and more uncut material, and the forces on the grain increases, reaching a maximum at the end, when the grain leaves the interface surface. So $\dot{Q}_F$ also varies as the cut progresses. Published results [27] indicate that of the three types of variations assumed, linear, parabolic, uniform, the last one gave fairly accurate results.

CHAPTER V

CONCLUSION AND FUTURE WORK

The present model for obtaining grinding temperatures and residual stresses using Finite Element Method yields good results. The temperatures that are obtained, are in good agreement with the published experimental results. The stress distribution that was obtained from these temperatures agrees with the results available in literature qualitatively.

The increase in the depth of cut and table speed results in,

(1) the peak value of the temperature to rise to such an extent that thermal damage to the ground surface in the form of grinding burn takes place.

(2) the peak value of the tensile residual stress to increase, finally reaching the ultimate strength of the material resulting in grinding cracks, thereby reducing the fatigue strength of the workpiece.

At lower table speed the depth of affected zone is increased, whereas at lower depth of cut, it decreases. Variation in the heat transfer coefficient, so as to simulate the effect of coolant, has marginal effect on the peak value of the tensile residual stresses. Therefore, for better grinding results, a lower depth of cut and table speed is preferable. Accuracy

of the results can be further improved by employing a finer mesh at the ground surface, and decreasing the step length of the wheel movement. The present model can be further strengthened by including the phase changes that take place on the ground surface, the heteroginity of the material. Further, to obtain realistic values by Finite Element Method, the input parameters such as the fraction of the grinding energy entering the workpiece, the variation of heat flux along the wheel-workpiece contact zone should be known exactly.

REFERENCES

1. Guest, J.J., "The theory of grinding'', Proc. Inst. Mech. Engnrs., 1915, pp. 71-73.

2. Outwater, J.O., Shaw, M.C., ''Surface temperatures in grinding'', Trans. ASME, J. of Engg. for Ind., Vol. 74, 1952, pp. 73-86.

3. Des-Ruisseaux, N.R., Zerkle, R.D., ''Thermal analysis of grinding process'', Trans. ASME, J. of Eng. for Ind., Vol. 92B, 1970, pp. 428-434.

4. Scrutton, R.F., Lal, G.K., ''Thermal analysis of the wear of single abrasive grains'', Trans. ASME, J. of Eng. for Ind., Vol. 96, 1974, pp. 1245-1251.

5. Jaeger, J.C., ''Moving sources of heat and temperatures of sliding contacts'', Proc. Roy. Soc. of New South Wales, Vol. 76, 1942, pp. 203-224.

6. Sato, K., ''Grinding temperatures'', Bull Japan Society of Grinding Engnrs., Vol. 1, 1961, pp. 31-36.

7. Malkin, S., Anderson, R.B., ''Thermal aspects of grinding'', Trans. ASME, J. of Engg. for Ind., Vol. 96, 1974, pp. 1239-1244.

8. Sauer, W.G., ''Thermal aspects of grinding'', Ph.D.Thesis, Carneigie Mellon University, Pittisburg, Pa., 1971.

9. Glikman, L.A., Sanfinova, T.P. and Stepanov, V.A., ''Origin of residual stresses in grinding of high chromium stainless steels'', J. Tech. Physics, Vol. 19, 1949, pp. 441.

10. Frisch, J. and Thomsen, E.G., ''Residual grinding stresses in Mild steel'', Trans. ASME, Vol. 73, 1951, pp. 337.

11. Marshell, E.R., and Shaw, M.C., ''Forces in dry surface grinding'', Trans. ASME, Vol. 74, Jan. 1952, pp. 51-59.

12. Letner, H.R., ''Residual grinding stresses in hardened steel'', Trans. ASME, Vol. 77, 1955, pp. 1089.

13. Letner, H.R., ''Influence of grinding fluids upon residual stresses in hardened steels'', Trans. ASME, Vol. 79, 1957, pp. 149.

14. Colwell, L.V., Sinnot, M.J., and Tobin, J.C., ''The determination of residual stresses in hardened and ground steel'', Trans. ASME, Vol. 77, 1955, pp.1099-1105.

15. Halverstadt, R.D., ''Analysis of residual stresses in ground surfaces of high temperature alloys'', Trans. ASME, Vol. 80, 1958, p. 928.

16. Denton, A.A., ''Determination of residual stresses'', Met. Reviews, Vol. 11, 1966, pp. 1-23.

17. Mishra, A., Rao, U.R.K., Natarajan, R., ''An analytical approach to the determination of residual stresses in surface grinding'', Proc. Int. Conf. on Prod. Engg., Vol. 2, 1977, pp. vi40-vi50.

18. Zienkiwicz, O.C., ''The Finite Element Method in Engineering Science'', McGraw Hill, London, 1971.

19. Huebner, K.H., ''The Finite Element Method for engineers'', John Wiley and Sons., U.S.A., 1975.

20. Heuser, J., ''Finite Element Method for thermal analysis'', NASA Rep TN D-7274, Nov., 1973.

21. Pande, S.J., Lal, G.K., ''Grinding wheel life and economics'', J. of Engg. Production, Vol. 4, 1981, pp. 18-30.

22. Ueda, Y., Yamakawa, T., ''Thermal stress analysis in metals with temperature dependent mechanical properties'', Proc. of Int. on Mech. Behaviours of Mat., Vol. III, 1971, pp. 10-20.

23. Mayer, J.E., Shaw, M.C., ''Grinding temperatures'', Lubrication Engineering, 1957, pp. 21-26.

24. Hahn, R.S., ''The relation between grinding conditions and thermal damage in workpiece'', Trans. ASME, J. of Engg. for Ind., Vol. 78, 1956, pp. 807-812.

25. 'Grinding stresses-cause, effect and control'', Collection of papers published by Grinding Wheel Institute of America, Cleveland, Ohio, 1961.

26. Hahn, R.S., ''On loss of surface integrity, surface form due to thermo-plastic stress in plunge grinding operation'', Annals of C.I.R.P., Vol. 25, 1976, pp. 203.

27. Snoeys, R., Luoven, K.U., Maris, M., Peter, B.J., ''Thermally induced damage in grinding'' Keynote paper, Annals of C.I.R.P., Vol. 27, 1978, pp. 571-581.

28. Tonshoff, H.K., Brinksmeier, E., ''Determination of mechanical and thermal influence of machined surface by micro-hardness and residual stress analysis'', Annals of C.I.R.P., Vol. 29/2, 1980, pp. 519-529.

29. Tonshoff, H.K., Brinksmeier, E., ''Optimisation of computer controlled X-ray stress analysis'', Annals of C.I.R.P., Vol. 30, 1981, pp. 509-513.

30. Cheung, Y.K., Yeo, M.F., ''A practical introduction to Finite Element Analysis'', Pitmann Publishing Ltd., London, 1979.

31. Martin, H.C., Carey, G.F., ''Introduction to Finite Element Analysis'', Tata McGraw Hill Publishing Co., New Delhi, 1979.

32. Desai, C.S., Abel, J.F., ''Introduction to Finite Element Method, A numerical method for engineering analysis'', Affliated East-West Press Pvt. Ltd., New Delhi, 1977.

APPENDIX

The workpiece is discretized into a finite number of Constant Strain Triangular elements as shown in Fig. Consider the figure shown below,

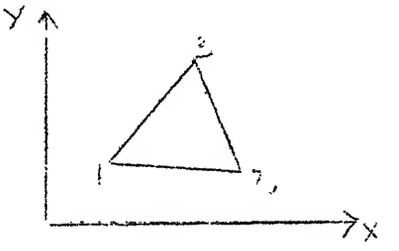

where 1,2,3 are the node numbers. The variation of the function (temperature or displacement) within this element is given by

$$\varphi^{(e)} = [\, N_1 \quad N_2 \quad N_3 \,] \begin{Bmatrix} \varphi_1 \\ \varphi_2 \\ \varphi_3 \end{Bmatrix}$$

where

$$N_1 = L_1 \, (2L_1 - 1)$$

$$N_2 = L_2 \, (2L_2 - 1)$$

$$N_3 = L_3 \, (2L_3 - 1)$$

The natural co-ordinates L_1, L_2, L_3 are related to the cartesian co-ordinates by

$$\begin{Bmatrix} L_1 \\ L_2 \\ L_3 \end{Bmatrix} = \frac{1}{2A^{(e)}} \begin{bmatrix} (x_2y_3 - x_3y_2) & (y_2 - y_3) & (x_3 - x_2) \\ (x_3y_1 - x_1y_3) & (y_3 - y_1) & (x_1 - x_3) \\ (x_1y_2 - x_2y_1) & (y_1 - y_2) & (x_2 - x_1) \end{bmatrix}$$

where x_i, y_i, $i = 1,2,3$ are the cartesian co-ordinates of node i. The area of the element $A^{(e)}$ is given by

$$A^{(e)} = \frac{1}{2}\begin{vmatrix} 1 & x_1 & y_1 \\ 1 & x_2 & y_2 \\ 1 & x_3 & y_3 \end{vmatrix}$$

The derivatives of the shape functions, which are used in assembling the stiffness matrices are given by

$$N_{1,x} = \frac{(y_2-y_3)}{2A^{(e)}} = \frac{b_1}{2A^{(e)}} \quad ; \quad N_{1,y} = \frac{-(x_2-x_3)}{2A^{(e)}} = \frac{C_1}{2A^{(e)}}$$

$$N_{2,x} = \frac{(y_3-y_1)}{2A^{(e)}} = \frac{b_2}{2A^{(e)}} \quad ; \quad N_{2,y} = -\frac{(x_3-x_1)}{2A^{(e)}} = \frac{C_2}{2A^{(e)}}$$

$$N_{3,x} = \frac{(y_1-y_2)}{2A^{(e)}} = \frac{b_3}{2A^{(e)}} \quad ; \quad N_{3,y} = -\frac{(x_1-x_2)}{2A^{(e)}} = \frac{C_3}{2A^{(e)}}$$

The thermal conductivity matrix for an element e is given by

$$[K_{TH}] = \frac{1}{4A^{(e)}}\begin{bmatrix} (k_x b_1^2+k_y c_1^2) & (k_x b_1 b_2+k_y c_1 c_2) & (k_x b_1 b_3+k_y c_1 c_3) \\ & (k_x b_2^2 + k_y c_2^2) & (k_x b_2 b_3+k_y c_2 c_3) \\ \text{SYM} & & (k_x b_3^2 + k_y c_3^2) \end{bmatrix}$$

Thermal capacitance matrix for an element is given by

$$[K_c] = \frac{\rho c A^{(e)} t^{(e)}}{12}\begin{bmatrix} 2 & 1 & 1 \\ 1 & 2 & 1 \\ 1 & 1 & 2 \end{bmatrix}$$

Material matrix, in Chapter 3 is given by

$$[C] = \begin{bmatrix} M_1 & M_1M_2 & 0 \\ M_1M_2 & M_1 & 0 \\ 0 & 0 & M_{12} \end{bmatrix}$$

where

$$M_1 = \frac{E(1-\nu)}{(1+\nu)(1-2\nu)} \quad ; \quad M_2 = \frac{\nu}{(1-\nu)}$$

$$M_{12} = \frac{M_1(1-M_2)}{2}$$

E = Young's Modulus; ν = poisson ratio

Matrix relating the stresses and strains is given by

$$[B] = \frac{1}{2A^{(e)}} \begin{bmatrix} b_1 & o & b_2 & o & b_3 & o \\ o & c_1 & o & c_2 & o & c_3 \\ c_1 & b_1 & c_2 & b_2 & c_3 & b_3 \end{bmatrix}$$

The stiffness matrix $[K_D]$ for an element is given by

$$[K_D] = \frac{t^{(e)}}{4A^{(e)}} \begin{bmatrix}
M_1 b_1^2 + M_{12} c_1^2 & & & & & \\
M_1 M_2 b_1 c_1 + M_{12} b_1 c_1 & M_1 c_1^2 + M_{12} b_1^2 & & \text{SYM} & & \\
M_1 b_1 b_2 + M_{12} c_1 c_2 & M_1 M_2 b_2 c_1 + M_{12} b_1 c_2 & M_1 b_2^2 + M_{12} c_2^2 & & & \\
M_1 M_2 b_1 c_2 + M_{12} b_2 c_1 & M_1 c_1 c_2 + M_{12} b_1 b_2 & M_1 M_2 b_2 c_2 + M_{12} b_2 c_2 & M_1 c_2^2 + M_{12} b_2^2 & & \\
M_1 b_1 b_3 + M_{12} c_1 c_3 & M_1 M_2 b_3 c_1 + M_{12} b_1 c_3 & M_1 b_2 b_3 + M_{12} c_2 c_3 & M_1 M_2 b_3 c_2 + M_{12} b_2 c_3 & M_1 b_3^2 + M_{12} c_3^2 & \\
M_1 M_2 b_1 c_3 + M_{12} b_3 c_1 & M_1 c_1 c_3 + M_{12} b_1 b_3 & M_1 M_2 b_2 c_3 + M_{12} b_3 c_2 & M_1 c_2 c_3 + M_{12} b_3 b_2 & M_1 M_2 b_3 c_3 + M_{12} b_3 c_3 & M_1 c_3^2 + M_{12} b_3^2
\end{bmatrix}$$